Fuel 307 (2022) 121768

Contents lists available at ScienceDirect

Fuel

journal homepage: www.elsevier.com/locate/fuel

Full Length Article

Ash transformation mechanism during combustion of rice husk and rice straw

Hossein Beidaghy Dizaji [a,b,*], Thomas Zeng [a], Hieronymus Hölzig [c], Jens Bauer [d], Gert Klöß [c], Dirk Enke [b]

[a] DBFZ Deutsches Biomasseforschungszentrum gemeinnützige GmbH, 04347 Leipzig, Germany
[b] Institute of Chemical Technology, Leipzig University, 04103 Leipzig, Germany
[c] Institute of Mineralogy, Crystallography and Materials Science, Leipzig University, D-04275 Leipzig, Germany
[d] Leibniz Institute of Surface Engineering (IOM), Leipzig, Germany

ARTICLE INFO

Keywords:
Silica-rich biomass combustion
Ash transformation
Thermodynamic equilibrium calculation
Ash viscosity
Crystallinity threshold

ABSTRACT

Biomass is an alternative energy resource to fossil fuels because of its potential to reduce greenhouse gas emissions. However, ash-related problems are serious obstacles for this development, especially for the use in combustion plants. Thus, design and operation of biomass boilers require detailed understanding of ash transformation reactions during thermochemical conversion. To evaluate ash transformation in silica-rich biomass fuels, rice husk and rice straw were selected because of their abundance, limited utilization conflicts with the food sector, as well as their potential in both energy and material applications. This paper reveals ash transformation mechanisms relevant for the ash melting behaviour of silica-rich biomass fuels considering chemical and phase composition of the ashes. In this regard, several advanced spectroscopic methods and diffractometry were employed to characterize the materials. The ash transformation reactions and the viscosity were simulated using thermodynamic equilibrium calculations and a slag viscosity modeling toolbox. The results illustrate the impact of impurities on the atomic structure of the silica resulting in an altered ash melting behaviour and viscosity of the silica-rich ashes. Chemical water washing, acid leaching, and blending of rice straw with rice husk strongly influenced the chemical composition of the ashes and improved ash melting behaviour. The analysis also revealed the correlation between the crystalline fraction and the porosity in silica-rich biomass ashes, as well as a crystallinity threshold. These findings are highly relevant for future investigations in boiler designs and production of biogenic silica for material applications.

1. Introduction

In short and mid-term perspective, greenhouse gas emissions as main driver of global warming and climate change will be restricted to fulfil ambitious national and international agreements [1,2]. The European Green Deal has already set the goal to achieve CO_2 neutrality by 2050 [3]. In order to meet the ambitious climate protection targets, biomass as a nearly CO_2-neutral energy resource needs to be considered to replace fossil fuels [4]. Biomass should also not compete with sustainable food supply or land use for the nutritional crops production, and it should be readily available [5]. Rice husk (RH) and rice straw (RS) as by-product of rice production fulfil these requirements [6–8]. RH and RS are widely available and their share in global agricultural residues is 43% [9]. According to the report of Food and Agriculture Organization of the United Nations (FAO), world paddy rice production increases continuously and it reached around 800 million tons in the recent years

Abbreviations: AC, Ash content; BE, Binding energy; BET, Brunauer-Emmett-Teller; Blended, Blended rice straw with rice husk; BO, Bridging oxygen; CF, Chemical fractionation; CHN, Elemental analysis for carbon, hydrogen, and nitrogen determination; db, Dry basis; EC, Elemental carbon; ESI, Electronic supplementary information; eV, Electron volt; highT ash, Ash which is produced at temperatures higher than 550 °C; LHV, Lower heating value; LOI, Loss on ignition; lowT ash, Ash which is produced at 550 °C; LRH, Acid-leached rice husk; LRS, Acid-leached rice straw; M, Metal; MC, Moisture content; NBO, Non-bridging oxygen; n.d., Not detected; nsa, non-slagged ash; OC, Organic carbon; RH, Rice husk; RS, Rice straw; RT, Residence time; sa, slagged ash; SSA, Specific surface area; SVMT, Slag viscosity modelling toolbox; TP, Temperature program; VM, Volatile matter; wb, Wet basis; WRH, Water-washed rice husk; WRS, Water-washed rice straw; wt.%, Weight percentage; Q^n, Status of Si atom in the atomic structure. The n value represents number of BO atoms bonded to the Si in the silica tetrahedron unit cells..

* Corresponding author at: DBFZ Deutsches Biomasseforschungszentrum gemeinnützige GmbH, 04347 Leipzig, Germany.
E-mail address: hossein.beidaghy@dbfz.de (H. Beidaghy Dizaji).

https://doi.org/10.1016/j.fuel.2021.121768
Received 22 April 2021; Received in revised form 6 July 2021; Accepted 18 August 2021
Available online 2 September 2021

[10]. Approximately 20–25 and 40–60 wt% of paddy rice are RH and RS, respectively, corresponding to a huge potential for bioenergy production [11,12]. Commonly, however, these residues are disposed by open field burning which causes regional environmental and carcinogenic health problems in rice harvesting areas [13–15]. However, under controlled combustion, a pure silica (i.e. biogenic silica) can be generated from RH and RS in addition to energy supply. High-quality silica has various industrial applications, such as adsorption of heavy metal ions, production of catalyst supports, zeolites, silica-based mesoporous material synthesis and drug delivery [16–20]. In addition, it can be employed in concrete production reducing the global CO_2 emissions in this sector [21–24]. However, for a specific application, the biogenic silica must fulfil dedicated requirements with respect to e.g. purity, crystallinity and porosity. Besides process related parameters, the composition of the biomass has a major impact and limitation of critical ash forming elements is pivotal to obtain biogenic silica with high purity and to avoid ash melting that can hamper silica quality [25–27].

Biomass is comprised of organic and inorganic materials [28]. The main organic compounds of the biomass are cellulose, hemicellulose, and lignin [29,30]. Besides the organic matter, the biomass contains varying amounts of ash forming elements such as: Si, Ca, Mg, K, Na, P, S, Cl, Al, Fe, Mn, and some trace elements [31,32]. Ash chemistry involves complex interactions of ash forming elements, and during thermochemical conversion of the biomass, association of the ash forming elements can cause ash melting problems [32].

Studies of the ash chemistry can be simplified by excluding trace elements as well as Fe and Mn from the list of main ash forming elements [33]. Commonly, a system including K_2O, Na_2O, CaO, MgO, and SiO_2 is considered to investigate ash melting behavior of the biomass fuels. Since the characteristics of Na and Mg resemble to K and Ca, respectively, the behavior of Na and Mg can be approximated to those for K and Ca [33]. As a result, ash melting behavior of a phosphorus-poor biomass ash can be commonly evaluated with the three remaining compounds in the $K_2O(+Na_2O) - CaO(+MgO) - SiO_2$ ternary system [34–36]. It is believed that the role of P, especially its interaction with biomass ash melting, is less covered in literature [32,37–41]. In general, P is disregarded from the proposed biomass ash chemistry, particularly for biomass fuels with minor P content in their fuel ash. However, in the phosphorous-rich biomass fuels, critical melting compositions can be investigated with the help of the $K_2O(+Na_2O) - CaO(+MgO) - P_2O_5$ ternary phase diagram [32]. Phosphates remain in the bottom ash as stable crystalline phosphate and amorphous phosphosilicate phases [32].

To reduce ash related problems and to increase silica purity, water washing and acid leaching can be applied as an effective method to reduce the level of critical ash forming elements in silica-rich biomass assortments and employed strategies for the production of high quality biogenic silica have been reviewed recently [14]. Inorganic species of the solid fuels can be categorized into three groups [42]: (a) water-soluble share (i.e., alkali chlorides, carbonates, and sulphates, as well as the alkali earth chlorides), (b) acid soluble share (i.e., water-insoluble but acid-leachable minerals such as alkali earth sulphates, sulphides, and carbonates as well as the organically bounded species to the organic matrix), and (c) residual share (insoluble minerals such as silicates and covalently bounded elements to the organic matrix). With the help of chemical fractionation (CF), it is possible to reveal how different ash forming elements are associated in the biomass fuels [43,44]. CF is based on the selective leaching and applies increasingly aggressive solvents, i.e. water, ammonium acetate, and hydrochloric acid, respectively, to monitor solubility of each ash forming chemical species of the biomass fuel [36,43,45]. Consequently, information on the necessary pretreatment for the removal of critical ash forming elements with undesired influence on the ash melting behavior can be derived from CF. Furthermore, information on the potential release of volatile ash forming elements can be derived from CF. The water-soluble share of alkali metal is likely to be released during combustion forming particulate matter in the flue gas while the water-insoluble share of alkali metals will more likely contribute to ash transformation processes and ash melting phenomena. In chemical pre-treatment selection, environmental impact of the process should also be considered in large scale processes [14]. Therefore, simple tap-water washing can be more favorable than strong acid leaching processes as a pre-treatment of solid biofuels. Ash chemistry and ash melting tendency of different biomass assortments have been extensively investigated in the past [32,33,42,46–48]. In general, in silica-rich biomasses, K- and Ca-silicates (especially K-silicates) are the most common phases with lower melting points, which can cause ash melting problem [31,49,50]. Jenkins et al. [27] applied K_2O - CaO - SiO_2 ternary system to study ash melting behavior of original and pre-treated RS. They observed that pre-treatment shifts the composition to the silica corner of the ternary diagram with higher fusion temperatures (approx. 1500 °C), whereas, the untreated RS fused below 1000 °C. It was reported that the observed shift relates to the effect of pre-treatment on the concentration of alkali and alkaline earth elements in RS. The shift in the fusion temperature was also confirmed later by Yu et al. [51]. According to their investigation, untreated RS ash sintered at 1050 °C, and it completely melted at 1200 °C. In contrast, water washed RS started to fuse at 1550 °C. Although ash melting of silica-rich biomass fuels has been studied in literature, the ash quality cannot be predicted according to the available ash melting investigations.

Here, thermodynamic equilibrium calculations can provide a useful tool to simulate the ash transformation process. Several powerful software packages such as: ChemApp [52–54], ChemSheet [55], FactSage [56–58], HSC [59], MTDATA [60], Thermo-Calc and DICTRA [61] have been developed so far, which can model the ash chemistry. Lindberg et al. [62] reviewed all these software packages and databases, and they reported that FactSage is one of the most powerful tools to predict ash transformation reactions in biomass combustion. FactSage has also shown a promising potential to simulate ash transformation reactions in different biomasses [63].

A deeper understanding of the interdependency between ash transformation processes and the implied consequences for the slag formation risk and the viscosity of the formed slag would be highly valuable to support attempts to produce high quality biogenic silica from silica-rich biomass fuels for material applications.

In this paper, the ash chemistry of silica-rich biomass fuels has been investigated both experimentally and theoretically to i) reveal the impact of water washing and acid leaching on ash and mineral phase composition of untreated and pre-treated rice husk ash (RHA) and rice straw ash (RSA) at different temperatures, ii) elucidate the underlying reasons for low melting tendencies of several silica based mineral phases, iii) describe the impact of ash melting behavior (i.e. slag formation, structural and viscosity change) on the ash quality (i.e. silica purity, porosity and crystallinity of the ash) of silica-rich biomasses. This was done using different spectroscopic methods (i.e. SEM/EDX, XPS, and ICP-OES), as well as a quantitative diffractometric technique (i.e. XRD) accompanied and bolstered by thermodynamic equilibrium calculations.

2. Materials and methods

Fuel and sample preparation, ashing processes, solid fuel and ash analysis as well as thermodynamic equilibrium calculation and statistical analysis are described in the following subsections.

2.1. Fuels and sample preparation

RS and RH were purchased from Cascina Borella, Frazione Goido, 27,035 Mede, Pavia, Italy in the form of four round bales, each approx. 300 kg and nine big bags each approx. 150 kg, respectively. Ordinary tap water and citric acid (Sigma-Aldrich, Steinheim, Germany, purity of > 99.99%) were used as washing and leaching agents in chemical pre-

treatment of the fuels. Leaching was conducted in a solution of 1 wt% citric acid diluted with tap water. Commonly, stronger acids or higher acid concentrations are used in literature to modify the chemical composition of the RH and RS [64–68]. Alternatively, deionized water is also commonly employed for the pre-treatment of the RH and RS [64,65,67,69] which resulted in improved silica purity and higher ash porosity [14,68,70]. In order to minimize the cost and environmental impact of the chemical pre-treatment, tap water and an organic acid with low concentration were selected for water washing and acid leaching of the fuels. Fluorite (Sigma-Aldrich, Steinheim, Germany, purity of $>$ 99.9%) was employed as a reference material in XRD characterization and Rietveld refinement. Ashing was performed under constant air atmosphere while synthetic air flow was utilized for the thermogravimetric analysis, respectively.

Nine RH samples of approximately 2.5 kg of RH were collected from different levels and positions within each of the big bags using a tube sampler. Then, collected nine samples were combined for 20 min in a mixer to produce approx. 22.5 kg homogenized starting homogenized material. Furthermore, approximately 5 kg of RS were collected from each RS bale. Then, the collected four samples were merged together to have approx. 20 kg of RS. Collected RS was chopped using a mesh size of $<$ 5 mm, and it was subjected to the mixer for 20 min to merge the samples and to homogenize the RS as a starting material. In Table ESI.1.1 in ESI.1, the chemical pre-treatment conditions and designated sample labels are listed in detail. Water washed and citric acid leached rice straw and rice husk samples are labelled as WRS, LRS, WRH and LRH, respectively.

2.2. Ashing

Two different ashing processes were employed, i.e. low-temperature (lowT) ashing and high-temperature (highT) ashing as described in subsections 2.2.1 and 2.2.2.

2.2.1. LowT ashing

Low temperature (lowT) ashing is a strategy to remove the organic share of biomass fuels and to improve the homogeneity of the initial materials prior to the lab-scale experiments [63]. If the ashing process is employed in an uncontrollable manner, ignition may occur, and uncontrolled high temperatures may result in possible elemental losses [63]. Therefore, as shown in Fig. ESI.2.1 in section ESI.2, an adapted stepwise ashing temperature program (TP) which has been reported by Thy et al. [63] was applied using a muffle furnace with constant air atmosphere. A maximum ashing temperature of 550 °C was selected to burn the organic fraction of the biomass fuels, and at the same time to avoid crystallization of the ashes. According to the literature [14], untreated materials crystallized at temperatures between 600 and 900 °C depending on the source of the material and thermochemical conversion conditions. Crystalline silica is a source of carcinogenic health problems [71,72]. Therefore, ash crystallization should be shifted to higher conversion temperatures. The crystallization temperature shifts to higher values by chemical pre-treatment of silica-rich biomass fuels [70,73–76]. Therefore, selected maximum lowT ashing temperature secures the amorphous nature of the product. In each ashing test, 100 g (wet based) of each biomass fuel were ashed. It was repeated until enough lowT ash was produced from each of the biomass samples. In each experiment, the biomass was distributed as a thin layer into a big alumina crucible to have maximum air contact during the ashing. Generated lowT ashes were grinded with a mortar and sieved with a 0.5 mm cubic mesh and homogenized manually. Then, the homogenized lowT ashes were characterized as described in section 2.3.2, and used as the starting material in highT ashing, described in section 2.2.2.

2.2.2. HighT ashing

In the highT ashing procedure of the homogenized lowT ashes, a thermal treatment at 600, 700, 800, 900, 1000 or 1100 °C was performed. For this process, a muffle furnace was employed with constant air atmosphere. The muffle furnace was heated up to the desired temperature and then, 0.5 g of lowT ashes were subsequently placed into the furnace for 4 h. In these experiments, 20 ml conical crucibles made of Alsint 99.7 wt% with maximum withstand temperature of 1700 °C were used. Designated ash sample labels in highT ashing are presented in Table 1. In each individual experiment, the cooling process was performed using liquid nitrogen to quench the ash sample and prevent further chemical reactions or further conversion. To cool the samples, the crucibles were transferred immediately after highT ashing into a flask with liquid nitrogen. After cooling, the samples were kept in a dryer at 105 °C in order to prevent any adsorption of ambient moisture into the pore structure of the ashes. Then, the ashes were sieved using multiple cubic mesh sizes (3.15, 2, 1, and 0.5 mm). Finally, the ash particles with sizes$>$3.15 mm were separated as the slagged (or partially slagged) particles in each individual ash, and this fraction was analyzed separately. The remaining ash fractions were combined and analyzed as non-slagged ash particles. Slagged and non-slagged ashes were indicated by “sa” and “nsa” in the result section. The sieving and slag categorization were performed based on the PASSA method [77,78]. For the porosity, chemical composition analysis, as well as the viscosity calculation, another 0.5 g of the homogenized lowT ashes were employed, and highT ashing were applied. Then, the generated highT ashes were analyzed without sieving.

Table 1
Sample nomenclature.

Run	Material	Biomass designation	Ash designation	RS	RH
1	Rice straw	RS	RSA	100	–
2	Rice husk	RH	RHA	–	100
3	50 wt% db rice straw-50 wt% db rice husk	Blended	Blended	50	50
4	Water washed rice straw	WRS	WRSA	100	–
5	Water washed rice husk	WRH	WRHA	–	100
6	Acid leached rice straw	LRS	LRSA	100	–
7	Acid leached rice husk	LRH	LRHA	–	100

2.3. Analysis

Analysis section includes different solid fuel and ash analysis as described in the following subsections.

2.3.1. Solid fuel analysis

Proximate and ultimate fuel analysis were carried out for the untreated and chemically pre-treated fuels according to the existing standards for solid biofuels [79] regarding moisture content (MC), ash content (AC), volatile matter (VM), elemental composition (CHN), total content of S and Cl as well as major and minor elements. The procedure of sample preparation for the ICP-OES analysis is described in ESI.3. The composition of the ash forming elements in the fuel was determined on the fuel ash, which was prepared at 550 °C according to the standard procedure [80]. CF was carried out on solid fuels according to the literature [81]. Details of the CF procedure are presented in Fig. ESI.4.1 in ESI.4.

2.3.2. Ash analysis

In order to confirm complete decomposition of the organic share of the solid biomass fuels (untreated or pre-treated biomass fuels) during the lowT ashing, the ashing process was studied using a Simultaneous Thermo-gravimetric Analysis (STA 449 F3 Jupiter®, NETZSCH, Germany) coupled with Quadrupole Mass Spectrometer (QMS 403 Aëolos Quadro, NETZSCH, Germany). The procedure was monitored under an identical lowT ashing TP as described in Fig. ESI.2.1 in section ESI.2. Heating rate, sample amount, and synthetic air flow rate were 10 K/min,

~10 mg, and 100 ml/min, respectively. Each of the biomass fuels was grinded with a cutting mill (IKA™ MF 10 basic Mikrofeinmühle) to a particle size below 0.5 mm and mixed vigorously in a plastic box to prepare homogeneous starting material for the STA-QMS analysis. To remove the flow effect from thermogravimetric (TG) curve, each experiment was performed in two steps. First, TG curve of an empty crucible was recorded by applying lowT-ashing TP. In the second step, the same crucible was filled with the biomass fuel and the TG was measured under the same TP. Finally, TG of the empty crucible was subtracted from the sample curve. In order to monitor the carbon dioxide evolution as well as the water evaporation, as the products of biomass combustion during the ashing process, ions with mass per charge (m/z) of 44 and 18 were monitored, respectively, with the QMS.

Carbon content of the lowT-RS and lowT-RH ashes were measured using EC/OC, elemental analysis (CHN), and Loss on Ignition (LOI) methods [82,83]. Water content of these ashes was determined using Karl-Fischer titration method [84]. Elemental-composition distribution of lowT-RS ash and the selected highT-RS ash were examined with a scanning electron microscopy-energy dispersive X-ray spectroscopy (SEM-EDX) in a Zeiss Gemini Ultra 55 machine with a Bruker XFlash 3001 detector. Prior to EDX analysis the sample was coated by a thin chromium film to avoid surface charging during the measurement. Acquisition time for EDX mapping of an 393 μm × 295 μm analysis field at 787 × 590 pixel resolution was 1.5 h. Beam accelerating voltage, magnification, beam aperture, and the working distance were 20 KV, 500x, 60 μm, and 8.5 mm, respectively. Mean EDX count rate and the estimated EDX spot size were 15.5 kcps and 1.2 μm. For composition evaluation and enhanced data analyses as phase recognition the Bruker ESPRIT 2.2 software is used. $Cr_{K\alpha}$ and $C_{K\alpha}$ are included in the peak deconvolution, but they are excluded for composition calculation.

Quantitative crystalline phase determination of both the lowT and highT ashes was realized by XRD analysis and by using the Rietveld refinement method [85,86]. The samples were measured in a BRUKER D8 Discover (Bruker AXS Advanced X-ray Solutions GmbH, Karlsruhe) with $Cu_{K\alpha}$ radiation (1.5418 Å) and a VÅNTEC-500 2D detector in the range of 15° to 65° in 2θ. Each experiment comprised 3 frames and a measuring time of 3600 s. The 2D diffractograms were integrated and evaluated using DIFFRAC.EVA V 3.1 software and PDF-2 2002 database. The mass fractions of crystalline phases were quantified via Rietveld refinement using TOPAS software. The crystalline fraction of the ashes was quantified with respect to a crystalline reference material, which was standard calcium fluorite.

Chemical composition of highT-RS sample was also determined using a surface sensitive XPS (Kratos Ultra DLD) at room temperature. A cross-section of freshly broken piece of the slagged ash was analyzed in XPS in order to prevent any contamination on the chemical composition of the studied sample. Analysis spot size was 700 × 300 μm^2. The measurement was performed with monochromatic excitation of $Al_{K\alpha}$ radiation (150 W, hϑ=1486.6 eV), as the X-ray source. The photoelectron yield is enhanced applying a magnetic immersion lens. Detail spectra corresponding to each inclusive chemical element were obtained after scanning at a pass energy (PE) of 40 eV with step width of 0.1 eV. A charge neutralization was carried out to eliminate shifted binding energy arising from non-conductive sample charging. BE was calibrated based on C 1 s with BE = 285.0 eV. UNIFIT 2021 software package [87] was employed to evaluate XPS experimental data and determine the areas corresponding to each element considering the specific transmission correction of the XPS machine. For curve fitting convolved Gaussian-Lorentzian peak profiles are simultaneously optimized with a Shirley background profile.

Gas sorption of the ashes was performed using Autosorb iQ apparatus (Quantachrome) and liquid nitrogen as the operating gas at 77 K. Multipoint Brunauer-Emmett-Teller (BET) was employed to measure BET specific surface area (BET SSA). BET SSA was determined in the pressure range of p/p_0 = 0.05–0.3, considering cross-section area of nitrogen molecules of 16.2 Å [88,89]. Prior to the gas sorption method, samples were degassed and activated under ultrahigh vacuum for 12 h at 250 °C [65,90].

Content of major and minor elements in the fuel ashes were determined according to DIN EN ISO 16967:2015–07 [91] using an inductively coupled plasma with optical emission spectrometer (ICP-OES) after HF digestion. Details of the measurement and the obtained results are presented in ESI.3. Viscosity of the ashes was calculated according to the slag viscosity modelling toolbox (SVMT) presented by Duchesne et al. [92]. For these calculations, chemical composition of the ashes obtained from the ICP-OES analysis were utilized.

Crystallographic structure of the presented species was visualized using VISTA 3.0 software package [93].

2.4. Thermodynamic equilibrium calculation

Using FactSage 8.0 software package, thermodynamic equilibrium calculations were performed to predict phase composition of the remaining ashes. In the FactSage software, the chemical equilibrium is calculated considering the Gibbs energy of all phases and minimizing the total Gibbs energy of the whole chemical system [57]. In this regard, equilibrium module and FToxid, FTsalt and FactPS databases (version 2020) were employed to get thermodynamic information about the oxides, salts, and pure elements in gaseous, liquid and solid states [57]. According to the report of Lindberg et al. [62], FToxid database presented by Pelton et al. [58,94] provides the most comprehensive data for solid and liquid silicates and oxides. Elemental chemical composition of the solid fuels (fuel ash composition) obtained by ICP-OES was inserted to the software as the input data. Pressure of the ash transformation reactions as well as the excess air ratio were set to 1 atm and λ = 1. The temperature was monitored between 550 and 1100 °C by 50 K intervals. The combustion air was assumed to be an ideal gas. FToxid-SLAGB was also chosen as the solution phases in the calculation. Duplicated gases, liquids and solid species have been deselected and removed from the calculations by applying the priority for the databases as "FToxid, FTsalt, FactPS" [95]. Therefore, for the similar chemical species, data were obtained from FToxid, FTsalt or FactPS, respectively.

3. Results

3.1. Solid fuel analysis

Table 2 presents the result of fuel analysis including proximate and ultimate analysis, as well as the lower heating value of the fuels and chemical composition of the fuel ash.

According to the Table 2, all untreated and chemically pre-treated biomass fuels are characterized by an ash content of approx. 13–15 wt % db. Washing of the biomasses with water increased the silica content of RS and RH ashes from 69.78 and 89.66 to 87.07 and 93.60 wt% db, respectively. Thermal treatment of the acid leached fuels yielded biogenic silica with a purity of 90.70 (RS) and 97.72 wt% db (RH). Observed silica enrichments are in agreement with the literature data [14].

As shown in Table 2, K, Ca, Mg, P and S are the most abundant ash forming elements beside Si in RS. Whereas, the major ash forming elements except Si in RH are K and Ca, respectively. The behavior of listed ash forming elements in sequential CF process is displayed in Fig. 1.

Fig. 1 shows the share of water soluble, ammonium acetate or hydrochloric acid leachable, as well as the non-leachable fraction of the ash forming elements. In RS, Fig. 1a, K is generally water soluble, and only limited amount of K remains in the solid residue as non-soluble share. Water washing can also remove a considerable fraction of Mg, Mn, Na, and P from RS. Ammonium acetate is not an effective leachate to remove the critical ash forming elements in RS. A significant fraction of Ca is acid leachable by HCl. The other elements (i.e. Si, S, Cl, Fe, and Al) remain generally in the solid residues as non-leachable elements. According to Fig. 1b, in RH, Ca, Na and K show higher solubility

Table 2
Fuel and fuel ash properties of RS, WRS, LRS, RH, WRH, and LRH. Inorganic species are specified on fuel ash basis. Abbreviations wb, db, and n.d. stand for wet basis, dry basis and not detected. Oxygen is calculated by difference.

	Fuel analysis						
Parameter	unit	RS	WRS	LRS	RH	WRH	LRH
MC	wt.% wb	7.55	4.28	4.82	11.20	2.57	2.76
AC	wt.% db	13.96	13.43	13.11	15.4	13.98	13.41
VM	wt.% db	71.80	74.86	75.14	67.21	71.86	73.24
LHV	MJ/kg db	15.87	16.69	16.87	15.80	16.36	16.55
C	wt.% db	42.80	42.70	43.30	42.40	42.80	42.70
H	wt.% db	5.33	5.26	5.33	5.12	5.20	5.07
N	wt.% db	0.74	0.50	0.50	0.46	0.37	0.39
O	wt.% db	50.47	51.44	50.76	51.84	51.58	51.78
S	wt.% db	0.09	0.07	0.08	0.05	0.04	0.04
Cl	wt.% db	0.57	0.03	0.03	0.13	0.01	0.02
	Fuel ash analysis						
Compound	unit	RS	WRS	LRS	RH	WRH	LRH
Al_2O_3	wt.% db	0.10	0.07	0.07	0.12	0.08	0.06
CaO	wt.% db	4.32	9.15	5.86	1.30	3.55	0.73
Fe_2O_3	wt.% db	0.20	0.24	0.28	0.12	0.16	0.09
K_2O	wt.% db	15.59	0.02	0.02	4.99	0.02	0.01
MgO	wt.% db	2.06	0.69	0.31	0.58	0.61	0.17
MnO	wt.% db	0.68	0.40	0.12	0.21	0.17	0.02
Na_2O	wt.% db	n.d.	n.d.	n.d.	n.d.	n.d.	n.d.
P_2O_5	wt.% db	1.88	0.62	0.49	0.96	0.69	0.40
SiO_2	wt.% db	69.78	87.07	90.70	89.66	93.60	97.72
SO_3	wt.% db	1.62	1.33	1.79	0.98	0.90	0.63
Others	wt.% db	0.08	0.18	0.09	0.06	0.13	0.04

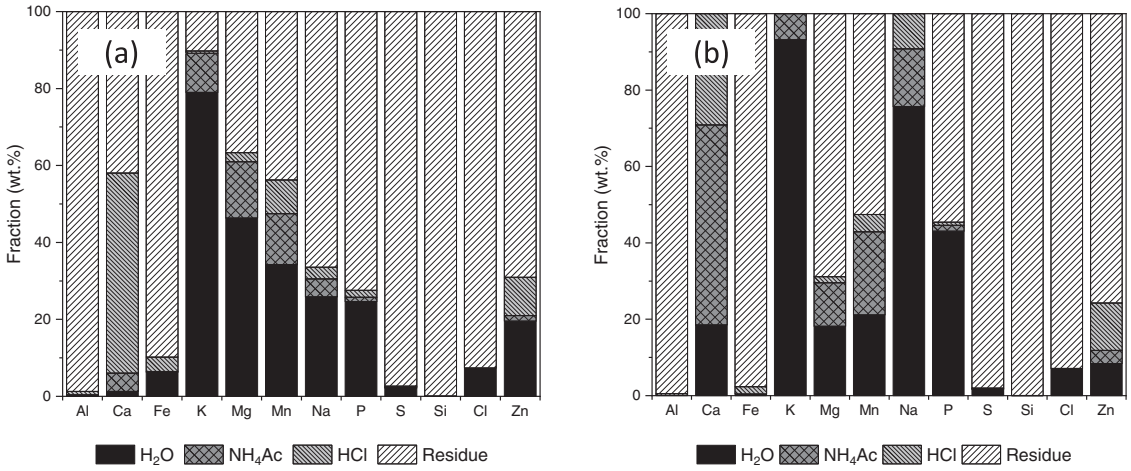

Fig. 1. Chemical fractionation results of (a) RS and (b) RH. Reported values are the average of three measurements.

compared to the RS. Consequently, these elements can be almost completely removed from the biomass during CF.

In CF, the remaining fraction of the ash forming elements in the solid residues can be attributed to the ash melting in the residual ashes.

3.2. Ash analysis

The results of lowT and highT ashing are presented in subsections 3.2.1 and 3.2.2.

3.2.1. LowT ash

As indicated in section 2.3.2, lowT ashing process was studied using a STA-QMS device. Results of the STA experiments, of the selected lowT ashes are illustrated in Fig. ESI.2.2 - Fig. ESI.2.7. The results showed that the investigated fuels decompose completely during the lowT ashing procedure, and lowT ashes are characterized by almost no carbon. Results from the analysis of the elemental composition and from the determination of the moisture content are compiled in Table ESI.2.1 and Table ESI.2.2 in ESI.2. Distribution of different chemical elements in lowT ashes is an important parameter which shows the accessibility of different chemical species and their contribution in the ash transformation reactions. Figure ESI.2.8 in ESI.2 shows the SEM-EDX mapping of different elements in lowT-RS ash. This sample was selected for chemical mapping, because it contains the highest amount of critical ash forming elements in its chemical composition (Table 2). As shown in Figure ESI.2.8 in ESI.2 , almost all the elements are highly distributed within the sample, and it confirms the homogeneity of the ash. Quantitative results from the EDX analysis for this sample are reported in Table ESI.2.3 in ESI.2.

3.2.2. HighT ash

Fig. 2 presents the results of Rietveld refinements of XRD measurements corresponding to RS, WRS, LRS, RH, WRH, LRH, and blended RS with RH ashes generated at different temperatures. For RS, WRS, LRS, RS blended with RH as well as RH, slagging was observed at higher temperatures.

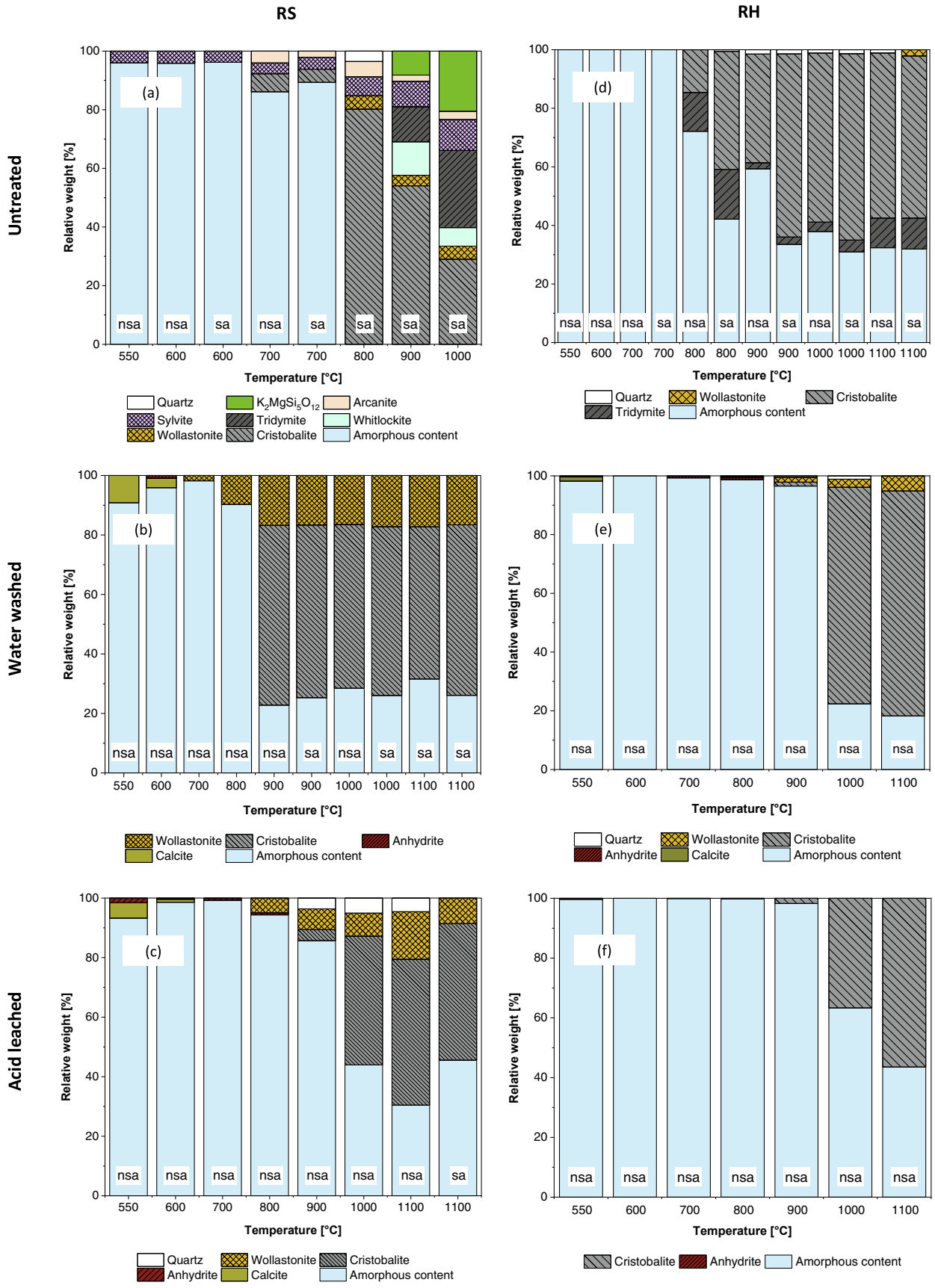

Fig. 2. Phase composition of (a) RS, (b) WRS, (c) LRS, (d) RH, (e) WRH, and (f) LRH, and (g) blended RS with RH ashes. Slagged/partially slagged (particle size > 3.15 mm) and non-slagged (particle size < 3.15 mm) ashes were indicated by "sa" and "nsa" labels.

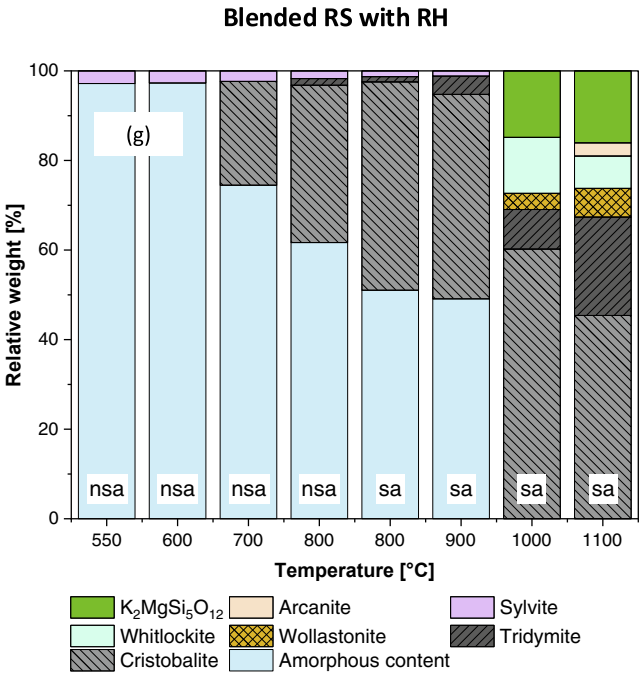

Fig. 2. (*continued*).

According to Fig. 2a, once the temperature increases from 550 to 700 °C, thermally non-stable phases, arcanite (K_2SO_4) and sylvite (KCl) remain in RS ash along with the crystallization of the previously amorphous silica. Formation of these phases was also reported in previous crystallographic investigations on different biomass assortments [30,32,34,46,47,96–99]. They were also observed in the blended RS with RH sample, Fig. 2g. In literature [100], formation of cristobalite and tridymite crystalline silica phases was observed at temperatures above 800 °C in RS ash, which is in agreement with the results of the XRD analysis. In general, the crystallization temperature depends on the phase composition of the silica-rich biomass [14]. Therefore, different crystallization temperatures were observed for RS and RH, Fig. 2a and Fig. 2d. According to the literature [14], pre-treatment shifts the crystallization of the ash to higher temperatures. In the present study, the crystallization temperature shifted from approximately 700 °C in RS and 800 °C in RH to 800–900 °C in WRS and LRS (Fig. 2a - Fig. 2c) and 900–1000 °C in WRH and LRH (Fig. 2d - Fig. 2f). This can be traced back to the reduction of the share of critical ash forming elements due to fuel pre-treatment. In general, the level of crystallization is high in the slagged ashes (sa, particle size bigger than 3.15 mm) compared to the non-slagged ones (nsa, particle size below 3.15 mm). LRH ashes are characterized by the lowest crystallinity degree at all studied temperatures. These samples have the highest share of amorphous content and silica purity.

In all pre-treated samples, except LRH ash, the fraction of wollastonite ($CaSiO_3$) is increased compared to the untreated biomass fuels, which is due to the increase in Ca level in the fuel ashes (Table 2). It might be due to the hardness of the tap water in the form of Ca^{2+} ions [101].

In WRS, LRS and WRH samples, calcite ($CaCO_3$) was observed at lower temperatures (550–600 °C). The reaction between CaO and ambient CO and CO_2 occurred after the heat treatment. It seems that this carbonate phase decomposed as CO and CO_2 at higher temperatures, and Ca reacted with SiO_2 at higher temperatures to form wollastonite.

In RS and blended RS with RH samples (Fig. 6a and Fig. 6d), at higher temperatures (approx. 900–1100 °C), whitlockite ($Ca_3(PO_4)_2$) and $K_2MgSi_5O_{12}$ were formed. Whitlockite is one of the most common phosphorus-based phases in biomass ashes [32,96,97,102]. $K_2MgSi_5O_{12}$

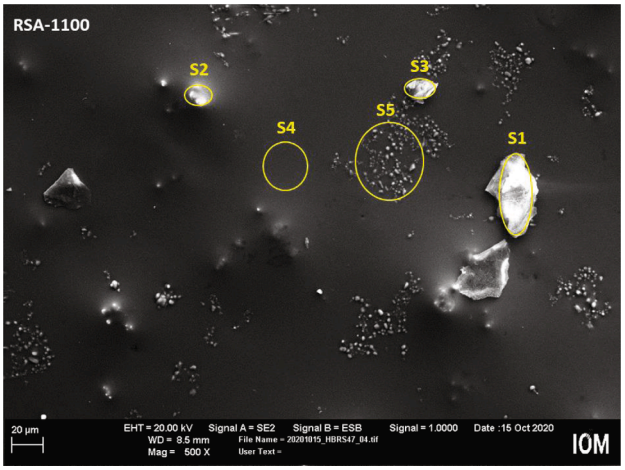

Fig. 3. Secondary electron (SE) image of RSA generated at 1100 °C recorded by SEM. Separated regions represents the selected areas for EDX analysis.

was also detected as a possible chemical phase in biomass ash in literature in both experimental [103] and simulation [104,105] results. Ma et al. [106] characterized this phase using XRD in RS ash at temperatures higher than 750 °C as a glassy compound. According to the report of Niu et al. [103], $K_2MgSi_5O_{12}$ can be formed at higher temperatures by arcanite, magnesium oxide, and silica in association with SO_2 release (equation 1).

Fig. 2a does not include phases corresponding to the rice straw ash (RSA) generated at 1100 °C (RSA-1100). It is because of high ash melting tendency of RSA at higher temperatures. At 1100 °C, a glassy ash was formed, and it covered the RSA sample. Visual inspection of RSA-1100 was performed, see Fig. ESI.5.1 in ESI.5. X-ray diffraction pattern of this samples is affected by the covering of glassy material, which is depicted in Fig. ESI.5.2 in ESI.5. Therefore, SEM-EDX and XPS analysis (presented in ESI.5) were carried out to determine the chemical composition of RSA-1100. Fig. 3 shows the SEM image of RSA-1100 in which the marked areas were selected for EDX mapping. Quantitative

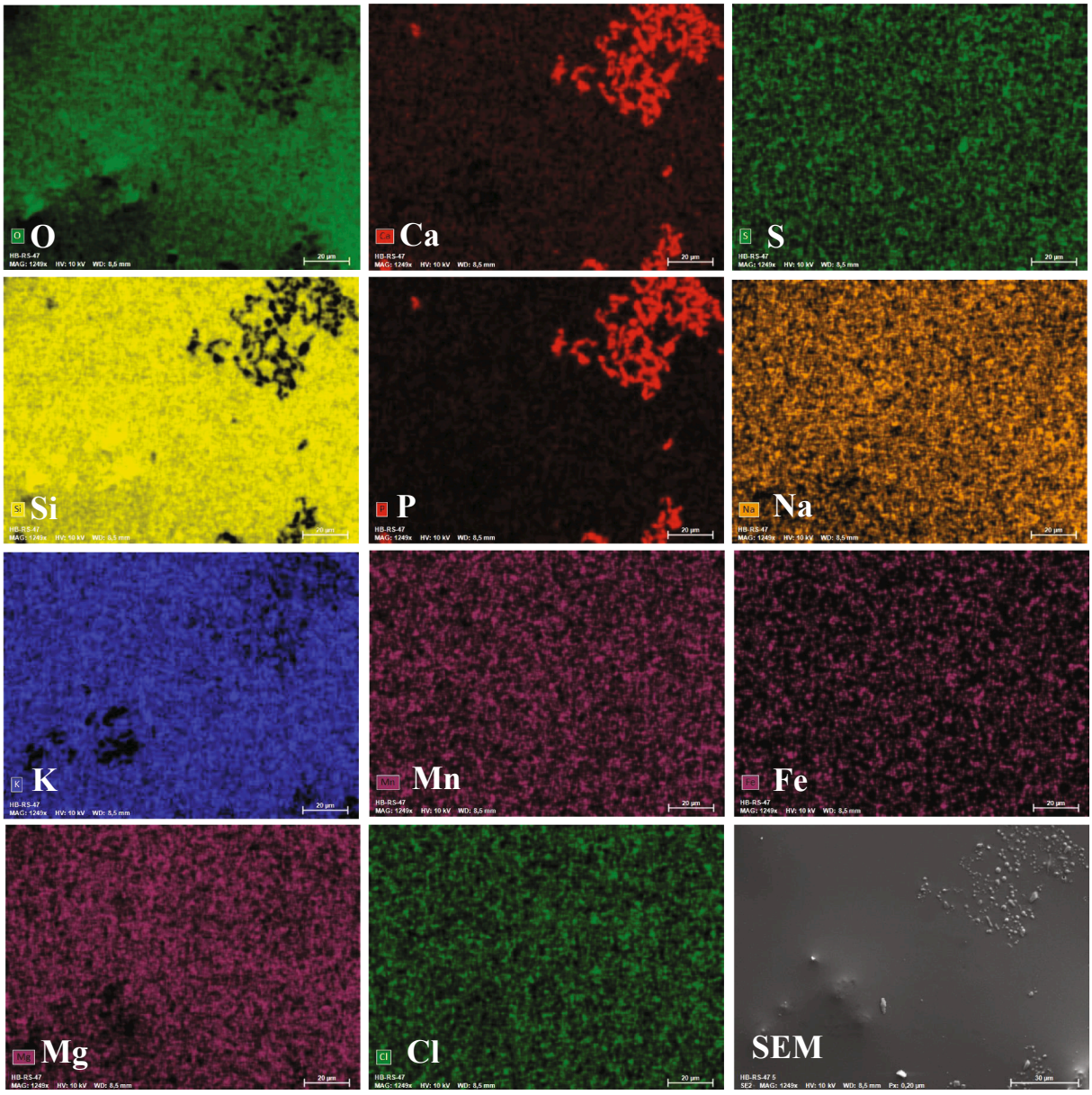

Fig. 4. EDX mapping of region labelled S5 corresponding to the sample RSA-1100.

EDX analysis results of the selected regions are presented in Table ESI.5.1 in ESI.5.

$$2K_2SO_4 + 2MgO + 10SiO_2 \rightarrow 2K_2MgSi_5O_{12} + 2SO_2 + O_2 \quad (1)$$

Two distinct morphologies can be differentiated for RSA-1100 in Fig. 3 (spots labelled S4 and S5). A graphical image of the EDX analysis was derived for these spots (S4: Fig. ESI.5.3 in ESI.5 and S5 in Fig. 4). As shown in these figures, Si and O are ubiquitous in all the mapping areas. It can be an indication for the silica phase. However, K is also highly distributed at the same regions where Si and O exist. There are also areas which are separated from the other regions which contain elevated concentration of Ca and P and very low concentration of Si compared to the other regions. This is a confirmation for the expected whitlockite phase, which was also observed in simulation and XRD phase analysis of RSA treated at a lower temperature (RSA-1000, Fig. 2a).

Fig. 5 shows an elemental overlay image in the presented mapping area (S5, presented in Fig. 3) using the Bruker ESPRIT 2.2 software. Quantitative composition of the selected regions, labelled as 1, 2, 3, and 4, are presented in Table ESI.5.2 in ESI.5. In the area number 1, a lower Si content and a higher concentration of P as well as Ca compared to the whole mapped area was found. It could be a further indication for the presence of whitlockite. Area number 2 is characterized by increased S and K content and diminished Si content compared to the whole mapped area. It can be an evidence for the expected arcanite phase besides the silica. Area number 3 has almost no other elements than Si representing a pure silica composition. The area number 4, which is highly distributed in all the mapped area, generally contains Si, O and K.

In order to evaluate the porosity evolution during the ash transformation process, BET SSA of the ashes obtained from different temperatures was determined (Fig. 6). An increased conversion temperature resulted in a decreased porosity for all samples. Above 900 °C, regardless of the chemical composition, the obtained ashes are non-porous materials. According to Fig. 6, when the temperature is below 900 °C, ash porosity generally depends on the chemical composition. Untreated RS has the lowest porosity among the investigated ashes at all temperatures. Blending RS with RH not only improves the ash melting behavior but it also increases the ash quality in terms of the ash porosity. However, the fuel blending provides limited potential while chemical pre-

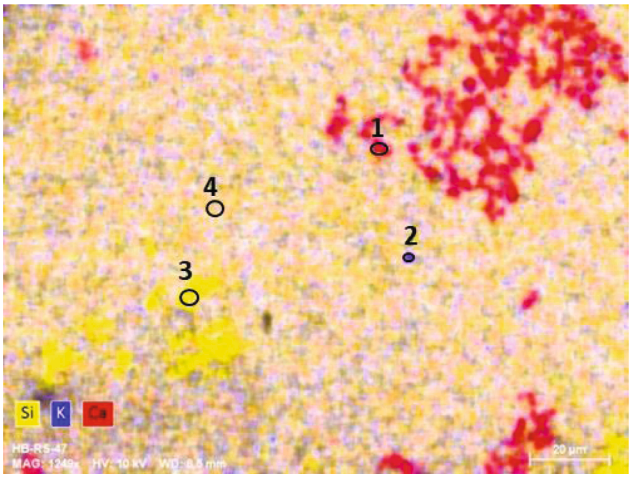

Fig. 5. Color-coded element overlay map of the region labelled S5 corresponding to the sample RSA-1100 using the Bruker ESPRIT 2.2 software. Composition of the selected regions (i.e. number 1–4) are presented in Table ESI.5.2 in ESI.5.

treatment (i.e. washing with water or citric acid) is more suitable to improve BET SSA which was also reported in the literature [70,73–76,107]. It is because the chemical pre-treatment decreases critical ash forming elements such as K resulting in decreased slag formation in the ash slagging tendency and higher BET SSA in non-slagged silica-rich ashes. Thus, according to Fig. 6, LRH, LRS, WRH, and WRS ashes are characterized by the highest porosities.

To study time dependency of phase and porosity changes at higher temperatures, lowT-LRH, with highest silica purity among the investigated ash samples, was subjected to different residence times (RT = 0, 1, 2, 3, 4, 5, and 240 min) at 1100 °C, and the chemical composition and the porosity changes were analyzed as shown in Fig. 7a and Fig. 7b. According to Fig. 7a, porosity of the LRH ash decreases upon prolonged heat treatment, and it drops to almost zero within 4 min. However, as illustrated by Fig. 7b, there is a time delay in ash phase transformation. It starts after 3 to 4 min of heat-treatment and it reaches chemically equilibrium condition after approximately 5 min.

According to Table ESI.6.1 in ESI.6, Shaw model [92,108], which is a modified Arrhenius equation introduced from an empirical fitting of data to relate viscosity of silicates to the temperature and ash melting characteristics, provides the best correlation between the BET SSA and crystallinity degree of the ashes among the applied viscosity models. Therefore, Shaw model was selected for calculation of the ash viscosities which were plotted as a function of temperature. The result is illustrated in Fig. 8, and is in accordance with reported viscosity data of different silicates [109]. It can be seen from Fig. 8 that RS has the lowest viscosity levels even at lowT ashing temperature and hence more severe slagging in the ash. Therefore, blending the RS with RH increases the viscosity of RS ash. However, pre-treatment is a more effective strategy to further increase the viscosity in both RS and RH samples.

3.3. Thermodynamic equilibrium calculations

Fig. 9 displays the results of thermodynamic equilibrium calculations using the FactSage 8.0 software. The simulations present phase changes of RS, WRS, LRS, blended RS with RH, RH, WRH, and LRH ashes from 550 to 1100 °C regardless of the crystallinity or amorphous nature of the reported phases. The combustion temperature is important factor on slag formation since a higher combustion temperature shall reflect a different heat treatment of the lowT ashes. According to Fig. 9, in the untreated biomass fuels, slag is formed and its share increases with higher combustion temperatures. Direct comparison of Fig. 9a and Fig. 9g reveals that blending of RS with RH improves ash melting behavior of the RS due to the change in chemical composition of the ash. However, blending cannot prevent the slag formation completely. Thus, water washing and acid leaching are more effective, Fig. 9b and Fig. 9c. Pre-treatment, does not only mitigate the ash melting problem, but it also improved the silica purity. In WRS and LRS, at higher temperatures, $CaSiO_3$ is the only dominant impurity of the ashes. In WRH and LRH samples, illustrated in Fig. 9e and Fig. 9f, the level of $CaSiO_3$ is very low due to the lower level of Ca in the fuel ash of the WRH and LRH compared to Ca level in WRS and LRS.

As shown in Fig. 9, unstable phases such as KCl, K_2SO_4, $CaSO_4$ are formed at lower temperatures, which diminished during the ash transformation process at higher temperatures. In the untreated and blended samples, at higher temperatures, SiO_2, $CaSiO_3$, $Ca_3(PO_4)_2$ and $K_2MgSi_5O_{12}$ are prevailing stable phases, which are in line with the XRD results. According to the results, there is a shift in the silica phase from SiO_2 (s1) to SiO_2 (s2) at around 870 °C, i.e. from quartz to tridymite,

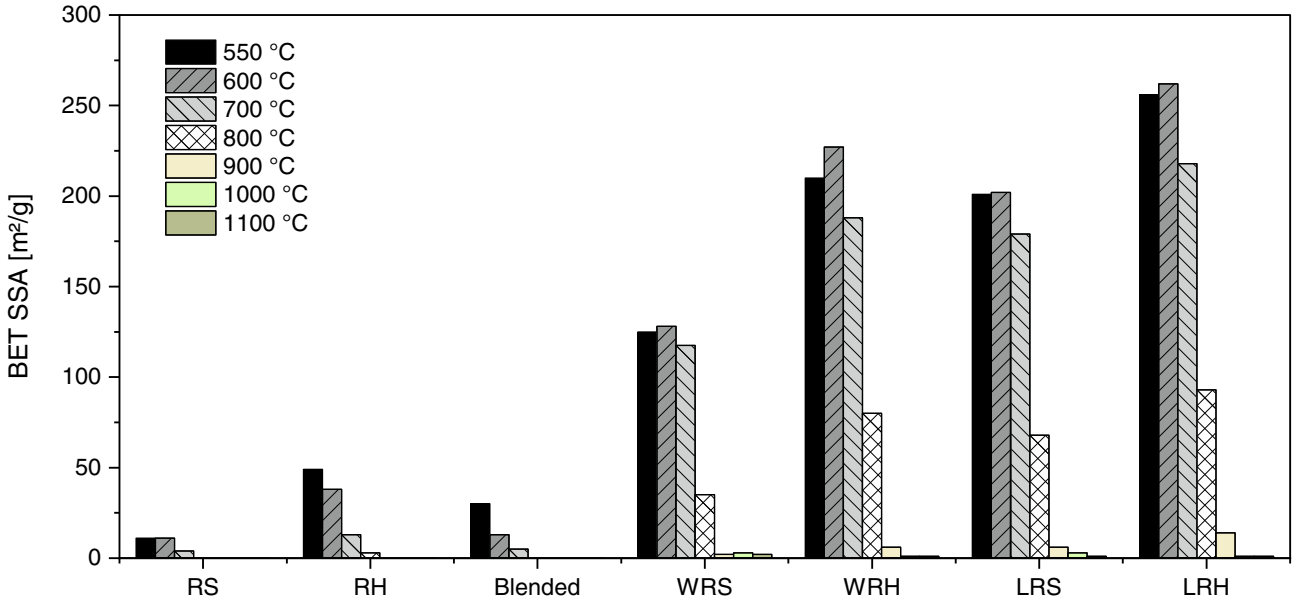

Fig. 6. BET SSA of the ashes produced at different temperatures.

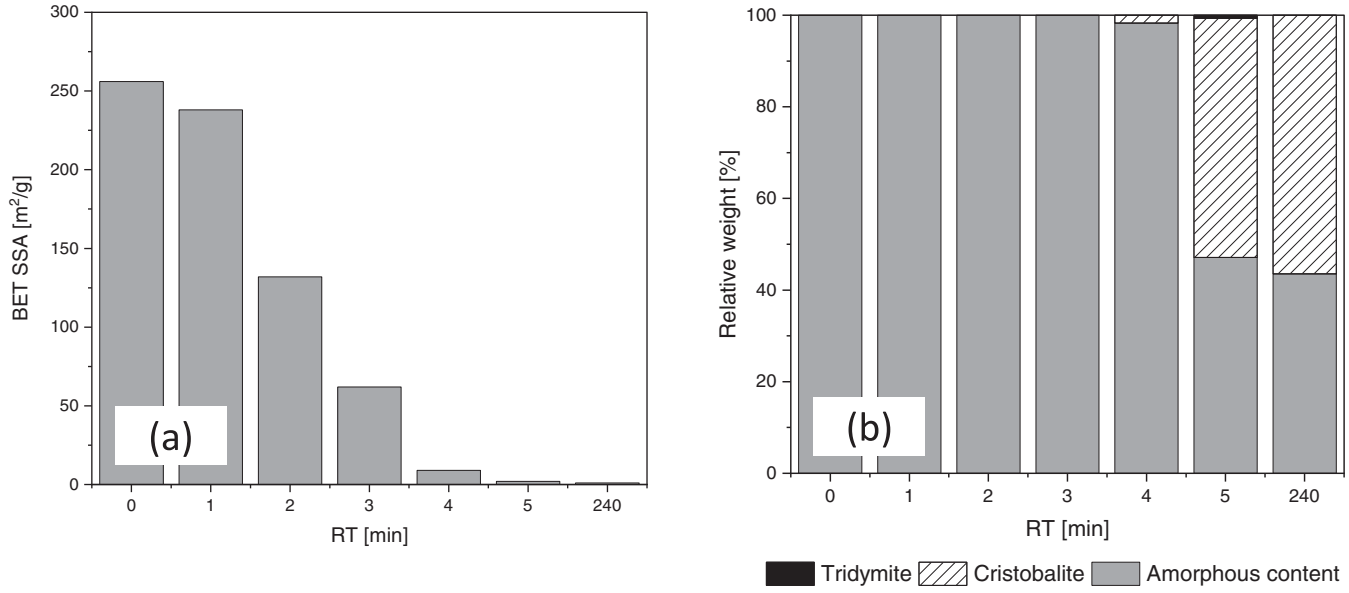

Fig. 7. (a) BET SSA and (b) phase changes of LRH ash sample as a function of RT at 1100 °C. RT = 0 and RT = 240 min represent lowT-LRHA and highT-LRHA, respectively.

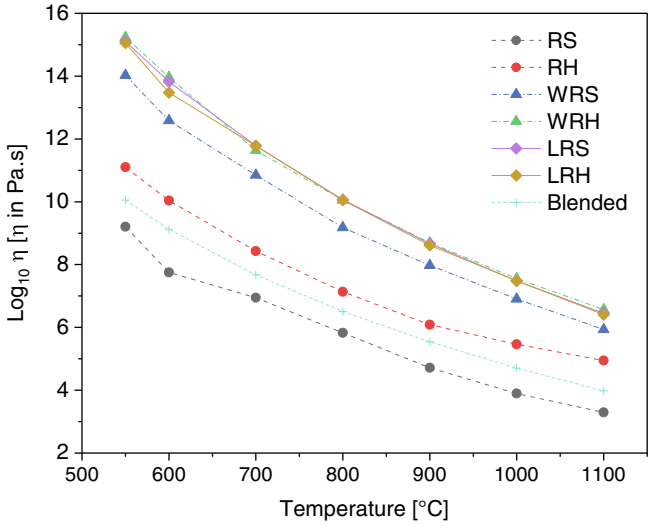

Fig. 8. Viscosity as a function of temperature in different ashes.

respectively. However, in the experimental results derived from XRD analysis, cristobalite is the dominating silica phases at elevated temperatures instead of tridymite, might be due to rapid cooling of the ash samples in liquid nitrogen after the heat treatment (see section 2.2).

Chemical composition of the slag phase is also crucial to understand the ash chemistry during the combustion. The thermodynamic equilibrium calculations provide an elemental composition of the slag phase. Table ESI.7.1 in ESI.7 displays the slag content and the elemental composition of the slag in RS, blended RS with RH and RH samples. The results show that Si, O, and K are the dominant elements in the slag composition.

In general, the ash chemistry of untreated biomass fuels is dominated by the distribution between different forms of silica and the slag phase (K-silicates). The other phases are relevant mainly at lower temperatures, and they are significantly reduced by water washing and acid leaching.

4. Discussion

Based on the results presented in section 3, in the following four subsections, evaluation of the data as well as the impact of the ash melting behavior on the structural changes, ash chemistry, porosity, crystallinity and the ash viscosity will be discussed.

4.1. Evaluation of analytical data and simulation results

In order to understand the ash melting behavior, phase composition of the ashes is an important aspect. The XRD measurement is limited to characterize only the crystalline phases in the ash samples. On the other hand, the thermodynamic equilibrium calculation is a powerful tool to simulate both crystalline and amorphous phases. However, in thermodynamic equilibrium calculation, kinetics of the ash transformation reactions does not play a role and crystalline and amorphous structures cannot be distinguished. Furthermore, in reality, there are also uncertainties about the mixing status as well as homogeneous spatial distribution of the ash forming elements, atmosphere and combustion temperatures within the fuel bed. Therefore, the results of Rietveld refinements in XRD and FactSage calculation should be considered simultaneously since each of these methods acts as a complementary approach for the other one. Therefore, only crystalline phases obtained from Rietveld refinements can be compared with those from FactSage calculations even though FactSage does not differentiate between crystalline and amorphous phases. According to the results, there is a good agreement between the results of XRD analysis, displayed in Fig. 2, and the FactSage calculations, presented in Fig. 9. However, there are also some differences, in particular with respect to the presence of unstable phases at higher temperatures which were detected in highT-ashes (e.g. arcanite and sylvite) while their formation was not predicted in FactSage simulation.

Nguyen et al. [100] visualized the chemical composition of the accumulated siliceous phytolith in RS, which is the deposited form of Si in rice plants, using X-ray tomographic microscopy. They observed that critical ash forming elements, K in particular, are trapped inside closed holes in the phytolith structure during plant growing period. Consequently, such ash forming elements cannot be removed even with severe leaching procedures and remain in the fuel ash (Fig. 1a). In the present study, chemical elemental mapping of lowT-RSA, as shown in

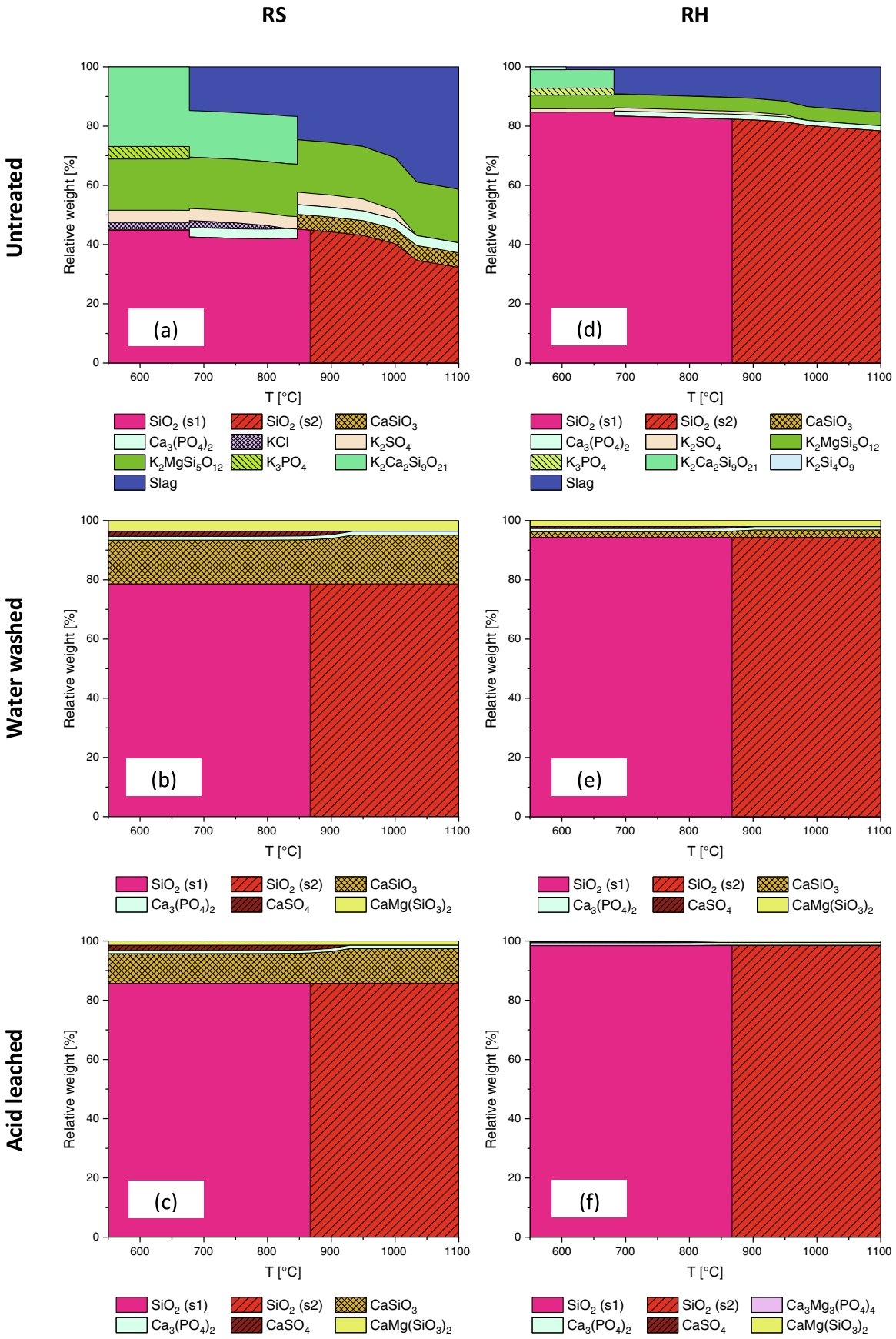

Fig. 9. Calculated phase composition of (a) RS, (b) WRS, (c) LRS, (d) RH, (e) WRH, (f) LRH, and (g) blended RS with RH ashes during heat treatment from 550 to 1100 °C.

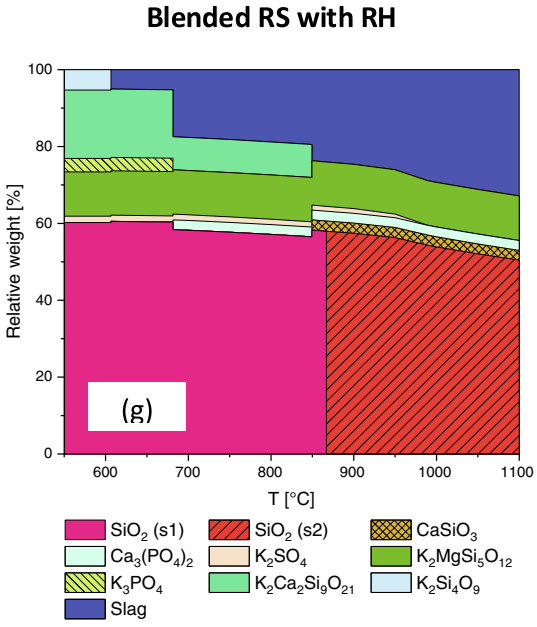

Fig. 9. (*continued*).

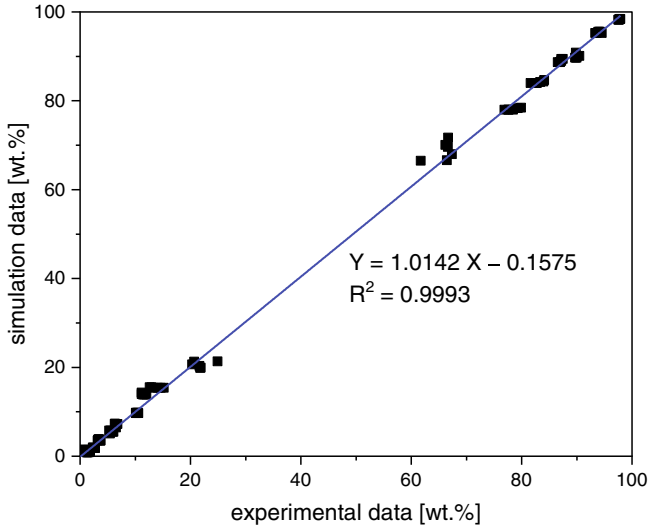

Fig. 10. Correlation between the ash composition obtained by ICP-OES and simulated by FactSage.

Fig. ESI.2.8 in ESI.2, also confirms that the ash forming elements such as K, S, and Cl are ubiquitous in the ash structure and they are distributed in contact with Si and O atoms. Consequently, arcanite and sylvite, are formed in the position where the silica network is growing during the ash transformation process. Therefore, considering the kinetic differences between the porosity evolution and the ash phase transformations, it is more probable that arcanite and sylvite are trapped in collapsed internal porosity structures once they are formed during the ash transformation reactions. As a result, they have been detected via XRD in RS ash at higher temperatures (Fig. 2a). In contrast, thermodynamic equilibrium calculations could not predict the formation of these phases at higher temperatures since only thermodynamically stable phases are displayed while unstable phases are considered to decompose at higher temperatures (Fig. 9a).

Comparison of ICP-OES results for the fuel ashes (listed in Table ESI.8.1 in ESI.8) with the ash composition from the thermodynamic equilibrium calculations (presented in Table ESI.8.2 in ESI.8)

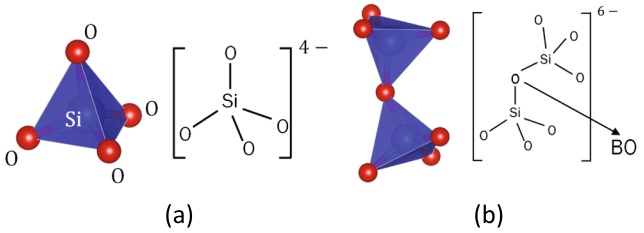

Fig. 11. Sketch of (a) a tetrahedral structural building unit of silica, and (b) silica tetrahedral unit network.

could be used to verify to which extent FactSage correctly predict the release of volatile ash forming elements. Fig. 10 shows the linear correlation (Y = AX + B) between the experimental and simulated data. The X-value of each dot in this figure represents the weight percentage of a specific element in a specific sample at a particular temperature measured by ICP-OES (see Table ESI.8.1 in ESI.8) The Y-value of the same dot is the weight percentage of the same element in the same sample at the same temperature calculated by the FactSage software (see Table ESI.8.2 in ESI.8).

Determination of the chemical composition of RSA-1100 using ICP-OES, XPS, and EDX techniques as well as the FactSage simulation provided comparative results (Table ESI.9.1 in ESI.9). Both surface sensitive techniques EDX and XPS reported lower Si levels as compared to the ICP-OES analysis of the bulky ash sample and simulation data. It indicates that there are different levels of the critical ash forming elements on the surface as compared to the bulk of the ash, which is in line with the report of Zareihassangheshlaghi et al. [65]. Thus, the ashes are characterized by a higher concentration of structure modifiers and critical phases (e.g. K-silicate) on the surface compared to the bulk.

4.2. *Structural changes and the ash chemistry*

In order to reveal the ash melting tendency and its initiation in silica-rich biomass ashes, the atomic structure of the pure biogenic silica prior to and after its crystallization should be considered. Fig. 11a shows an SiO_4^{4-} tetrahedron as the fundamental building unit of both crystalline and amorphous silica, with its 4 oxygen atoms bridging with further

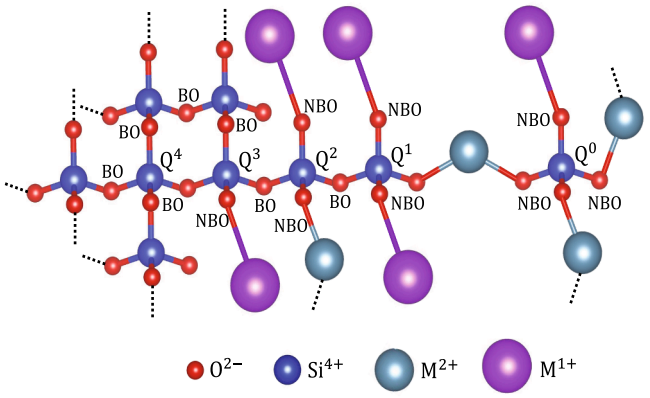

Fig. 12. Schematic of the silica network modifications by the metal (M) cations as the structural charge compensators.

silicon atoms of surrounding tetrahedra (Fig. 11b). The oxygen atom between the two silicon atoms together (Si-O-Si) with highly covalent metal–oxygen bonds is called bridging oxygen (BO) [110,111]. In amorphous silica the tetrahedral units link together randomly without a long range arrangement [112]. As a result, a random based porosity is formed inside the silica structure with a high free energy and low density. However, once the temperature increases and passes the crystallization temperature, the tetrahedral building units connect together with a long-range order. The crystalline structure of quartz, cristobalite, and tridymite are presented in Fig. ESI.10.1 in ESI.10. The melting temperature of pure silica is about 1710–1750 °C, which is a very high temperature [98,113–116]. It is probably because of strong network between the silica tetrahedral units, and the strong covalent bonds between Si and O atoms.

Since the silica units are negatively charged, they also have higher affinity to attract positively charged metal ions such as the metal cations K, Ca and Mg, to be electronegativity balanced. As shown in Fig. 12, different metal cations can be attracted by the silica tetrahedral units. Double charged cations (i.e., Ca^{2+} or Mg^{2+}) can be located between two oxygen atoms in the silicate network (i.e., Si-O-Ca-O-Si or Si-O-Mg-O-Si). Despite the similarities in the crystal structures, the newly formed crystals are less stable compared to pure silica. As a result, ash melting temperature of the newly formed phases (i.e., wollastonite) is lower than quartz, cristobalite, or tridymite. For instance, the ash melting temperature of wollastonite is around 1540 °C [116–121], and this temperature is 1557 °C for enstatite with chemical formula of $MgSiO_3$ [98].

If the attracted cation is an ion with single positive charge (i.e., K^+ or Na^{2+}), the cation acts as a network modifier and it breaks the silica network, as displayed in Fig. 12. These structures have comparatively low ash melting temperature compared to the pure silica phases or phases formed by double charged cations. For example, the melting point of K_2SiO_3 is 976 °C [121]. The oxygen which binds a silicon atom to a metal cation (i.e., Si-O-K or Si-O-Na) is called non-bridging oxygen (NBO) [110,122]. Each silicon atom in the newly formed atomic structures can also be identified as Q^n. Here, the value n indicates the number of BO atoms bonded to the Si in the silica tetrahedron unit cells [123,124].

The silica structure can be modified by a mixture of both alkali and alkaline earth metal cations. The melting temperature in this case will be in between the abovementioned two types of the silicates (e.g. melting point of $K_2MgSi_5O_{12}$ is between 1000 and 1100 °C [125] and this temperature is 1392 °C for diopside with chemical formula of $CaMg(SiO_3)_2$ [98].

Since the crystalline structures of both cristobalite and tridymite have a lower density and provide better possibility for the transportation of modifier cations as compared to quartz, modifier cations can more easily move through their crystal structures and form different phase incorporations with cristobalite and tridymite [126]. Fig. ESI.10.1 in ESI.10 presents crystal structures of quartz, cristobalite and tridymite viewed along the a-axis and perpendicular to the b-axis and c-axis.

Phosphorus can also change the crystalline structure of silicates at higher temperatures. It can be displayed as PO_4^{3-} tetrahedron and consequently modifies the structural network of the silicate materials [122,127]. It is due to the presence of PO_4^{3-} as the main phosphate group linked to the organic structure of biomass fuels [37]. Organic phosphates are transferred to inorganic phosphates since they are not thermally stable even at mild combustion temperatures [37]. During the thermal conversion, inorganic phosphates can react with alkali and alkaline earth metals (i.e. K, Ca, and Mg) to form more stable mineral phosphate phases. Because of the similarities between the silica and phosphorus tetrahedron, the most probable modification is the substitution of these two species [128]. Therefore, in silica-rich ashes with a source of Ca, whitlockite ($Ca_3(PO_4)_2$) can form at higher temperatures. Whitlockite is one of the most common phosphorus-based phases in biomass ashes [32,96,97,102]. Formation of the whitlockite as a phosphate lowers the net ash melting temperature, although it is not apparent in the simulated slag composition in Table ESI.7.1 in ESI.7. It is associated to the double bond between P and one of the O atoms in the PO_4^{3-} tetrahedron, which is not as strong as the silica network structure [128]. Häggström et al. performed a detailed investigation on the role of phosphorus during the thermal conversion of agricultural residues. Accordingly, the structure of whitlockite contains other cations such as K as substitute for Ca. At higher conversion temperatures, Mg can also be present in the whitlockite as substitute for Ca by excluding some K from the structure [39]. Thus, alkali and alkaline earth metals can act as modifiers in the network structure of the phosphates once they have entered into the network lowering the melting point of the phosphate phases. During a high-temperature fixed bed combustion, the cation exchange is facilitated resulting in the formation of K, Ca, and Mg phosphates rather than the Ca phosphates which is commonly reported for fluidized bed combustion [129]. If the share of alkali and alkaline earth metals is too low in the fuel mixture, whitlockite can (partly) remain unchanged in the ash [129,130]. Considering the CF of both RS and RH (Fig. 1) which well reflects the effect of the employed pre-treatment, phosphorus remains in the solid residue at the end of the fractionation process, and it indicates that P can be contained in the bottom ash along with the ash transformation reactions. It is in line with the report of Boström et al. [32] on the behavior of P in biomass combustion. According to the XRD results, whitlockite is formed at higher temperatures in RS (Fig. 2a) and blended RS with RH (Fig. 2g) ashes, but it is not formed in RH ashes. It is because, in RH, the CF showed that Ca does not remain in the residual ash (Fig. 1b). As a result, Ca in RH is not involved in the bottom ash transformation reactions at higher temperatures, and consequently whitlockite is not formed even though P is available for its formation. FactSage simulation (Fig. 9a, Fig. 9d, and Fig. 9g) also confirmed that the formation of whitlockite is more likely in RS and blended RS with RH than its generation in RH.

According to Fig. 2a, in RS, wollastonite ($CaSiO_3$) with Q^2 atomic structure is formed at 800 °C, and it remains in highT-RSA at higher temperatures, which is in agreement with simulated data presented in Fig. 9a. Wollastonite was also reported in literature as a possible phase in different biomass ashes [32,63,96,103,131–133]. According to the proposed atomic network theory, wollastonite increases the total ash melting tendency because of low ash melting temperature compared to its base silica phases with Q^4 atomic structures.

The different association of K and Mg in RS and RH is reflected by the differences in phase composition of the corresponding ashes. In RS a fraction of K is water-insoluble. At higher temperatures, K and Mg react with the silica to $K_2MgSi_5O_{12}$ which is observed as a crystalline phase at higher temperatures in RS and blended RS with RH samples (Fig. 2a and Fig. 2g). $K_2MgSi_5O_{12}$ was also detected as a possible phase in biomass ash in literature in both experimental [103] and simulation [104,105]

results. Ma et al. [106] characterized this phase using XRD in RS ash at temperatures higher than 750 °C as a glassy compound. According to the report of Niu et al. [103], $K_2MgSi_5O_{12}$ can be formed at higher temperatures by silica and arcanite in association with SO_2 releases (equation 1).

As the melting point of $K_2MgSi_5O_{12}$ is between 1000 and 1100 °C [125,134], in RSA-1100 sample, it seems that this phase melts and covers the surface of the remaining ash. The same temperature range was also reported by Thy et al. [135] in ash transformation process of RS. According to their report, RS ash completely melted at 1075 °C, and above 1170 °C, an extensive bubbling was observed as well as glassy ash material was formed. However, their report was based on lowT-RSA (generated at 575 °C) densified to 50 mg pellets.

The observed formation of $K_2MgSi_5O_{12}$ is in line with the simulation results presented in Fig. 9a and Fig. 9g. In contrast, this phase was not observed in RHA (Fig. 2d). Since CF indicate a completely water-soluble K content of RH (see Fig. 1b), potassium is more likely to be released as volatile ash-forming species from the ash at higher temperatures and consequently no $K_2MgSi_5O_{12}$ formation is observed in RHA.

As shown in Table 2, the employed pre-treatment processes (defined in section ESI.1 and Table ESI.1.1) removed K from the fuel ash. As a result, $K_2MgSi_5O_{12}$ does not exist in WRS and LRS samples both in experimental and simulation results presented in Fig. 2b, Fig. 2c, Fig. 9b and Fig. 9c.

According to the results of FactSage calculations, for the untreated biomass ashes (Fig. 9a, Fig. 9d, and Fig. 9g), the other possible reason for the slag formation is decreasing the amount of $K_2Ca_2Si_9O_{21}$. It seems that at higher temperatures, this phase accelerates the formation of slag in the original biomass ashes. Ca reacts with P or Si to form $Ca_3(PO_4)_2$ or $CaSiO_3$, and the association of remaining K, Si, and O elements augments the slag content. Based on this scenario, slag composition is rich in K, Si, and O, which corresponds well with the simulated slag compositions (listed in Table ESI.7.1 in ESI.7) and the commonly reported K-silicates phases with lower melting points in conversion of silica-rich biomasses in literature [31,49,50]. According to the silica network theory, this composition can also be considered as a critical phase with lower ash melting temperature.

4.3. Impact on porosity and crystallinity

As shown in Fig. 2 and Fig. 6, crystalline fraction and BET SSA of the ashes are highly dependent on the temperature. It indicates that when the aim is to produce high-quality porous biogenic silica, the temperature of the conversion process should be precisely controlled. Since the temperature inside the biomass boilers can fluctuate with respect to time and spatial distribution [70], a detailed CFD simulation is required to control the quality of the final product in real silica-rich biomass boilers.

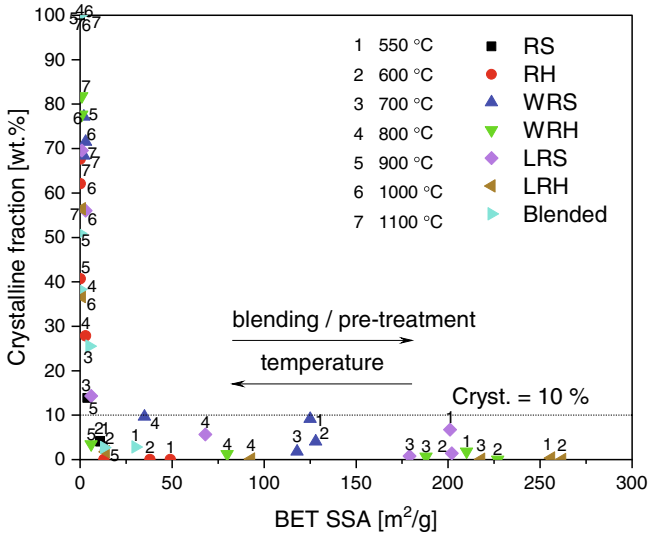

Fig. 13. Crystalline fraction vs. BET SSA in the ashes.

Fig. 13 displays the correlation between the crystalline fraction and BET SSA of the ashes. The correlation shows that there is a distinct threshold in crystallinity of the ashes (~10 wt% crystalline fraction). Above this, porosity of the ashes is suppressed by the crystallinity and, regardless to the temperature and the material composition, the result is a non-porous ash. However, below the crystallinity threshold, BET SSA increases by the blending and pre-treatment, and it is reduced with higher conversion temperature. Thus, the equilibrium condition of the presented experiments on the porosity changes is in the order of minutes which should be considered as crucial RT for boiler design [70].

Clustering of non-porous silica nanoparticles (ca. 4.2 nm in diameter) leads to a mesopore structure in silica [136]. At elevated temperatures the particles sinter together and the mesopores are diminished. Finally, the sintering results in a non-porous material. This process is accompanied by the crystallization of the ashes, which is shown in Fig. 13.

4.4. Impact on viscosity

The viscosity level of the ashes is completely in line with their ash melting tendency, and chemical pre-treatment increases the ash viscosity of both RS and RH, i.e. reducing problems due to slag formation. It is probably because of the improvement in silica purity level [137]. According to Fig. 8, a simple water washing of RH is sufficient to reduce water soluble elements (mainly K) and to avoid problems due to slag formation in the ash (i.e. resulting in high ash viscosity), which is almost equal to the viscosity of LRH ash. However, in RS, water washing is not sufficient to mitigate ash slagging (i.e. low ash viscosity), and acid leaching is required. In each ash material, higher conversion temperatures will result in a decreased ash viscosity, because critical phases with low ash melting temperature are formed. As mentioned in subsection 4.2, pure silica has strong silicon-oxygen bonds in a strong Q^4-type framework structure with maximum BO in the network, and this leads to higher ash viscosity (Fig. 8). Ma et al. [138] also showed a correlation between $(K_2O + CaO)/SiO_2$ ratio and the viscosity of the system, which was directly connected to structural changes in the system, where the variation of Si-O-Si angle or distance in silica network correlated with viscosity of the system. They calculated viscosity of the K_2O - CaO - SiO_2 system from a molecular dynamic simulation. However, their study was limited to the effect of K and Ca modifiers on the viscosity change of silica.

5. Conclusions

In this paper, ash transformation of silica-rich biomass fuels (i.e. rice husk and rice straw) was studied using both diffractometric and spectroscopic techniques, as well as the viscosity and thermodynamic equilibrium calculations. Chemical pre-treatment and blending of rice straw with rice husk were considered to mitigate the ash slagging risk of the rice straw and rice husk. Furthermore, these strategies improved the quality of the biogenic silica obtained after the combustion of these materials. According to the theoretical and experimental results, the following conclusions can be elucidated:

- For the first time, a threshold in crystallinity degree of the ashes (i.e. crystalline fraction ~ 10 wt%) was observed. In order to produce porous silica-rich ashes, crystalline fraction of the ash should be kept lower than the threshold value. Furthermore, the equilibrium conditions regarding to the porosity and crystallinity changes occur in the order of minutes. This information is highly relevant for the design of boilers.

- The ash chemistry of silica-rich biomasses revealed from the thermodynamic equilibrium calculations is in line with the experimental results obtained from XRD, ICP-OES, SEM-EDX, and XPS analysis. Linear correlation between the ash composition obtained from the simulation and the experiments showed a very good linear regression value ($R^2 = 0.9993$). Both the experimental investigation and the thermodynamic equilibrium calculations showed that after the combustion of untreated biomass fuels, K-, Mg-, and Ca-silicate, whitlockite, and other silica phases, as well as the slag are the dominant phases in the remaining ash, especially at higher combustion temperatures. For the combustion of chemically pre-treated samples, wollastonite is the only dominant phase beside the silica. However, the simulation was not able to predict the behavior of unstable phases such as KCl and K_2SO_4 due to the lack of kinetic considerations and other limitations of the thermodynamic calculation.
- Within the atomic structural model, the formation of different crystalline phases with lower melting points during the ash transformation of silica-rich materials can be described. According to the structural model, association of the silica network modifiers (alkali and alkaline earth metal cations), P, and Si cause the slag formation in the ashes at higher temperatures. Chemical fractionation can also supplement this model to predict the bottom ash related issues in biomass conversion.
- A time-dependent study revealed that Cl and S should not be disregarded from the chemistry of silica-rich ashes. In the present investigation, KCl and K_2SO_4, were observed in untreated rice straw ashes at elevated temperatures.
- The results of quantitative phase analysis as well as the ash porosity and viscosity investigations confirmed that blending of RS with RH modifies the ash composition and lowers the ash slagging risk. However, it is not sufficient to prevent the slag formation during highT-ashing process. The results showed that, chemical pretreatment is a better measure compared to the blending of the fuel in order to mitigate the ash melting problem.
- Association of P in the ash transformation mechanism and the structural change of RH and RS confirmed that this element should also be considered in future ash melting investigations on silica-rich biomasses.

Findings of the present paper are crucial to understand and mitigate the ash melting problem in silica-rich biomass combustion units. According to the results, in order to understand the ash chemistry and to control the slag formation in silica-rich biomass fuels, the role of different ash forming elements in the atomic structure of the ash should be considered.

CRediT authorship contribution statement

Hossein Beidaghy Dizaji: Conceptualization, Data curation, Formal analysis, Investigation, Methodology, Software, Visualization, Writing – original draft, Writing – review & editing. **Thomas Zeng:** Conceptualization, Methodology, Writing – review & editing, Funding acquisition. **Hieronymus Hölzig:** Methodology, Writing – review & editing. **Jens Bauer:** Methodology, Writing – review & editing. **Gert Klöß:** Methodology, Writing – review & editing. **Dirk Enke:** Conceptualization, Writing – review & editing.

Declaration of Competing Interest

The authors declare that they have no known competing financial interests or personal relationships that could have appeared to influence the work reported in this paper.

Acknowledgements

This work was financed by funds of the German Federal Ministry of Food and Agriculture (BMEL) based on a decision of the Parliament of the Federal Republic of Germany via the Federal Office of Agriculture and Food (BLE) under grant agreement number 2816DOKI03. Authors would like to express their sincere gratitude to the members of analytical and technical laboratories at German Biomass Research Centre (DBFZ) for their laboratory and technical supports in material preparation, analysis and characterizations. Special thanks to Dr. Jana Mühlenberg and Dr. Annett Pollex for their scientific comments as well as their advice in chemical fractionation of solid fuels. Authors would also like to express their appreciation to Professor Holger Kohlmann from Institute of Inorganic Chemistry in Leipzig, Germany and Dr. Peter Sommersacher from BEST-Bioenergy and Sustainable Technologies GmbH in Graz, Austria for their advice in XRD data analysis and thermodynamic equilibrium calculations, respectively. SEM and EDX data of the lowT-RS ash sample was recorded by Felix Meyerhöfer at Leipzig University, which is also appreciated.

Appendix A. Supplementary data

Supplementary data to this article can be found online at https://doi.org/10.1016/j.fuel.2021.121768.

References

[1] United Nations Framework Convention on Climate Change. Adoption of the Paris Agreement: Proposal by the President. Paris Climate Change Conference – November 2015, Cop 21, Paris. France.
[2] Bundesministerium für Umwelt, Naturschutz und Reaktorsicherheit (2016) Klimaschutzplan 2050: Klimaschutzpolitische Grundsätze und Ziele der Bundesregierung, Berlin, Germany.
[3] European Commission. Communication from the commission to the european parliament, the european council, the council, the european economic and social committee and the committee of the regions: The European Green Deal, COM/2019/640 final; 2019.
[4] Catuti M, Elkerbout M, Alessi M, Egenhofer C. Biomass and climate neutrality: CEPS Policy Insights, No 2020-19, August 2020.
[5] McKendry P. Energy production from biomass (part 1): Overview of biomass. Bioresource Technology 2002;83(1):37–46. https://doi.org/10.1016/S0960-8524(01)00118-3.
[6] Food and Agriculture Organization of the United Nations (FAO). Sustainable Rice Production for Food Security 2002 [Statistical Database]. Available online: http://www.fao.org/docrep/006/Y4751E/y4751e00.htm (accessed on 28 February 2021).
[7] Chen X-G, Lv S-S, Zhang P-P, Zhang L, Ye Y. Thermal destruction of rice hull in air and nitrogen. J Therm Anal Calorim 2011;104(3):1055–62. https://doi.org/10.1007/s10973-010-1201-2.
[8] Blissett R, Sommerville R, Rowson N, Jones J, Laughlin B. Valorisation of rice husks using a TORBED® combustion process. Fuel Process Technol 2017;159(8):247–55. https://doi.org/10.1016/j.fuproc.2017.01.046.
[9] Werther J, Saenger M, Hartge E-U, Ogada T, Siagi Z. Combustion of agricultural residues. Prog Energy Combust Sci 2000;26(1):1–27. https://doi.org/10.1016/S0360-1285(99)00005-2.
[10] Food and Agriculture Organization of the United Nations (FAO). Rice Market Monitor: April 2018. Available online: http://www.fao.org/3/I9243EN/i9243en.pdf (accessed on 28 February 2021).
[11] Chen H, Wang W, Martin JC, Oliphant AJ, Doerr PA, Xu JF, et al. Extraction of Lignocellulose and Synthesis of Porous Silica Nanoparticles from Rice Husks: A Comprehensive Utilization of Rice Husk Biomass. ACS Sustainable Chem. Eng. 2013;1(2):254–9. https://doi.org/10.1021/sc300115r.
[12] Kadam KL, Forrest LH, Jacobson WA. Rice straw as a lignocellulosic resource: Collection, processing, transportation, and environmental aspects. Biomass Bioenergy 2000;18(5):369–89. https://doi.org/10.1016/S0961-9534(00)00005-2.
[13] Lim JS, Abdul Manan Z, Wan Alwi SR, Hashim H. A review on utilisation of biomass from rice industry as a source of renewable energy. Renew Sustain Energy Rev 2012;16(5):3084–94. https://doi.org/10.1016/j.rser.2012.02.051.
[14] Beidaghy Dizaji H, Zeng T, Hartmann I, Enke D, Schliermann T, Lenz V, et al. Generation of high quality biogenic silica by combustion of rice husk and rice straw combined with pre- and post-treatment strategies—A review. Applied Sciences 2019;9(6):1083. https://doi.org/10.3390/app9061083.
[15] Wang W, Martin JC, Zhang N, Ma C, Han A, Sun L. Harvesting silica nanoparticles from rice husks. J Nanopart Res 2011;13(12):6981–90. https://doi.org/10.1007/s11051-011-0609-3.

[16] Chareonpanich M, Namto T, Kongkachuichay P, Limtrakul J. Synthesis of ZSM-5 zeolite from lignite fly ash and rice husk ash. Fuel Process Technol 2004;85(15): 1623–34. https://doi.org/10.1016/j.fuproc.2003.10.026.

[17] Foo KY, Hameed BH. Utilization of rice husk ash as novel adsorbent: A judicious recycling of the colloidal agricultural waste. Adv Colloid Interface Sci 2009;152 (1–2):39–47. https://doi.org/10.1016/j.cis.2009.09.005.

[18] He Q, Shi J. Mesoporous silica nanoparticle based nano drug delivery systems: Synthesis, controlled drug release and delivery, pharmacokinetics and biocompatibility. J. Mater. Chem. 2011;21(16):5845. https://doi.org/10.1039/C0JM03851B.

[19] Kwon S, Singh RK, Perez RA, Abou Neel EA, Kim H-W, Chrzanowski W. Silica-based mesoporous nanoparticles for controlled drug delivery. J Tissue Eng 2013; 4. https://doi.org/10.1177/2041731413503357. 2041731413503357.

[20] Liu D, Seeburg D, Kreft S, Bindig R, Hartmann I, Schneider D, et al. Rice Husk Derived Porous Silica as Support for Pd and CeO2 for Low Temperature Catalytic Methane Combustion. Catalysts 2019;9(1):26. https://doi.org/10.3390/catal9010026.

[21] Pode R. Potential applications of rice husk ash waste from rice husk biomass power plant. Renew Sustain Energy Rev 2016;53(3):1468–85. https://doi.org/10.1016/j.rser.2015.09.051.

[22] Rêgo JHS, Nepomuceno AA, Figueiredo EP, Hasparyk NP. Microstructure of cement pastes with residual rice husk ash of low amorphous silica content. Constr Build Mater 2015;80(9):56–68. https://doi.org/10.1016/j.conbuildmat.2014.12.059.

[23] Van V-T-A, Rößler C, Bui D-D, Ludwig H-M. Pozzolanic reactivity of mesoporous amorphous rice husk ash in portlandite solution. Constr Build Mater 2014;59(3): 111–9. https://doi.org/10.1016/j.conbuildmat.2014.02.046.

[24] Zain MFM, Islam MN, Mahmud F, Jamil M. Production of rice husk ash for use in concrete as a supplementary cementitious material. Constr Build Mater 2011;25 (2):798–805. https://doi.org/10.1016/j.conbuildmat.2010.07.003.

[25] Said N, Bishara T, García-Maraver A, Zamorano M. Effect of water washing on the thermal behavior of rice straw. Waste Manag 2013;33(11):2250–6. https://doi.org/10.1016/j.wasman.2013.07.019.

[26] Bakker RR, Jenkins BM, Williams RB. Fluidized bed combustion of leached rice straw. Energy Fuels 2002;16(2):356–65. https://doi.org/10.1021/ef010197w.

[27] Jenkins BM, Bakker RR, Wei JB. On the properties of washed straw. Biomass Bioenergy 1996;10(4):177–200. https://doi.org/10.1016/0961-9534(95)00058-5.

[28] Zhao X, Zhou H, Sikarwar VS, Zhao M, Park A-H, Fennell PS, et al. Biomass-based chemical looping technologies: The good, the bad and the future. Energy Environ. Sci. 2017;10(9):1885–910. https://doi.org/10.1039/C6EE03718F.

[29] Hartmann H. In: Encyclopedia of Sustainability Science and Technology. New York, NY: Springer New York; 2017. p. 1–36. https://doi.org/10.1007/978-1-4939-2493-6_245-3.

[30] Vassilev SV, Baxter D, Andersen LK, Vassileva CG, Morgan TJ. An overview of the organic and inorganic phase composition of biomass. Fuel 2012;94(3):1–33. https://doi.org/10.1016/j.fuel.2011.09.030.

[31] Kaknics J, Defoort F, Poirier J. Inorganic Phase Transformation in Miscanthus Ash. Energy Fuels 2015;29(10):6433–42. https://doi.org/10.1021/acs.energyfuels.5b01189.

[32] Boström D, Skoglund N, Grimm A, Boman C, Öhman M, Broström M, et al. Ash Transformation Chemistry during Combustion of Biomass. Energy Fuels 2012;26 (1):85–93. https://doi.org/10.1021/ef201205b.

[33] Näzelius I-L, Fagerström J, Boman C, Boström D, Öhman M. Slagging in Fixed-Bed Combustion of Phosphorus-Poor Biomass: Critical ash-forming processes and compositions. Energy Fuels 2015;29(2):894–908. https://doi.org/10.1021/ef502531m.

[34] Defoort F, Campargue M, Ratel G, Miller H, Dupont C. Physicochemical approach to blend biomass. Energy Fuels 2019;33(7):5820–8. https://doi.org/10.1021/acs.energyfuels.8b04169.

[35] Näzelius I-L, Boström D, Rebbling A, Boman C, Öhman M. Fuel indices for estimation of slagging of phosphorus-poor biomass in fixed bed combustion. Energy Fuels 2016;31(1):904–15. https://doi.org/10.1021/acs.energyfuels.6b02563.

[36] Zevenhoven M, Yrjas P, Skrifvars B-J, Hupa M. Characterization of ash-forming matter in various solid fuels by selective leaching and its implications for fluidized-bed combustion. Energy Fuels 2012;26(10):6366–86. https://doi.org/10.1021/ef300621j.

[37] Hedayati A, Lindgren R, Skoglund N, Boman C, Kienzl N, Öhman M. Ash Transformation during Single-Pellet Combustion of Agricultural Biomass with a Focus on Potassium and Phosphorus. Energy Fuels 2021;35(2):1449–64. https://doi.org/10.1021/acs.energyfuels.0c0332410.1021/acs.energyfuels.0c03324.s001.

[38] Lindström E, Sandström M, Boström D, Öhman M. Slagging characteristics during combustion of cereal grains rich in phosphorus. Energy Fuels 2007;21(2):710–7. https://doi.org/10.1021/ef060429x.

[39] Häggström G, Hannl TK, Hedayati A, Kuba M, Skoglund N, Öhman M. Single pellet combustion of sewage sludge and agricultural residues with a focus on phosphorus. Energy Fuels 2021;35(12):10009–22. https://doi.org/10.1021/acs.energyfuels.1c0088210.1021/acs.energyfuels.1c00882.s001.

[40] Wu H, Castro M, Jensen PA, Frandsen FJ, Glarborg P, Dam-Johansen K, et al. Release and transformation of inorganic elements in combustion of a high-phosphorus fuel. Energy Fuels 2011;25(7):2874–86. https://doi.org/10.1021/ef200454y.

[41] Grimm A, Skoglund N, Boström D, Öhman M. Bed agglomeration characteristics in fluidized quartz bed combustion of phosphorus-rich biomass fuels. Energy Fuels 2011;25(3):937–47. https://doi.org/10.1021/ef101451e.

[42] Niu Y, Tan H, Hui S'e. Ash-related issues during biomass combustion: Alkali-induced slagging, silicate melt-induced slagging (ash fusion), agglomeration, corrosion, ash utilization, and related countermeasures. Progress in Energy and Combustion Science 2016;52:1–61. https://doi.org/10.1016/j.pecs.2015.09.003.

[43] Zevenhoven-Onderwater M, Blomquist J-P, Skrifvars B-J, Backman R, Hupa M. The prediction of behaviour of ashes from five different solid fuels in fluidised bed combustion. Fuel 2000;79(11):1353–61. https://doi.org/10.1016/S0016-2361(99)00280-X.

[44] Werkelin J, Skrifvars B-J, Zevenhoven M, Holmbom B, Hupa M. Chemical forms of ash-forming elements in woody biomass fuels. Fuel 2010;89(2):481–93. https://doi.org/10.1016/j.fuel.2009.09.005.

[45] Zevenhoven-Onderwater M, Öhman M, Skrifvars B-J, Backman R, Nordin A, Hupa M. Bed Agglomeration Characteristics of Wood-Derived Fuels in FBC. Energy Fuels 2006;20(2):818–24. https://doi.org/10.1021/ef050349d.

[46] Vassilev SV, Baxter D, Vassileva CG. An overview of the behaviour of biomass during combustion: Part II. Ash fusion and ash formation mechanisms of biomass types. Fuel 2014;117(3):152–83. https://doi.org/10.1016/j.fuel.2013.09.024.

[47] Mlonka-Mędrala A, Magdziarz A, Gajek M, Nowińska K, Nowak W. Alkali metals association in biomass and their impact on ash melting behaviour. Fuel 2020;261 (2):116421. https://doi.org/10.1016/j.fuel.2019.116421.

[48] Reinmöller M, Schreiner M, Guhl S, Neuroth M, Meyer B. Ash behavior of various fuels: The role of the intrinsic distribution of ash species. Fuel 2019;253:930–40. https://doi.org/10.1016/j.fuel.2019.05.036.

[49] Gilbe C, Öhman M, Lindström E, Boström D, Backman R, Samuelsson R, et al. Slagging Characteristics during Residential Combustion of Biomass Pellets. Energy Fuels 2008;22(5):3536–43. https://doi.org/10.1021/ef800087x.

[50] Strandberg A, Skoglund N, Thyrel M, Lestander TorbjörnA, Broström M, Backman R. Time-Resolved Study of Silicate Slag Formation During Combustion of Wheat Straw Pellets. Energy Fuels 2019;33(3):2308–18. https://doi.org/10.1021/acs.energyfuels.8b04294.

[51] Yu C, Thy P, Wang L, Anderson SN, VanderGheynst JS, Upadhyaya SK, et al. Influence of leaching pretreatment on fuel properties of biomass. Fuel Process Technol 2014;128:43–53. https://doi.org/10.1016/j.fuproc.2014.06.030.

[52] Eriksson G, Königsberger E. FactSage and ChemApp: Two tools for the prediction of multiphase chemical equilibria in solutions. Pure Appl Chem 2008;80(6): 1293–302. https://doi.org/10.1351/pac200880061293.

[53] Petersen S, Hack K. The thermochemistry library ChemApp and its applications. Int J Mater Res 2007;98(10):935–45. https://doi.org/10.3139/146.101551.

[54] Eriksson G, Spencer P. A general thermodynamic software interface. Lehrstuhl Theoretische Huttenkunde, RWTH Aachen. Germany:115–26 1995.

[55] Bréchet Y, editor. Microstructures, Mechanical Properties and Processes - Computer Simulation and Modelling. Weinheim, FRG: Wiley-VCH Verlag GmbH & Co. KGaA; 2000.

[56] Bale CW, Chartrand P, Degterov SA, Eriksson G, Hack K, Ben Mahfoud R, et al. FactSage thermochemical software and databases. Calphad 2002;26(2):189–228. https://doi.org/10.1016/S0364-5916(02)00035-4.

[57] Bale CW, Bélisle E, Chartrand P, Decterov SA, Eriksson G, Gheribi AE, et al. FactSage thermochemical software and databases, 2010–2016. Calphad 2016;54: 35–53. https://doi.org/10.1016/j.calphad.2016.05.002.

[58] Bale CW, Bélisle E, Chartrand P, Decterov SA, Eriksson G, Hack K, et al. FactSage thermochemical software and databases — recent developments. Calphad 2009; 33(2):295–311. https://doi.org/10.1016/j.calphad.2008.09.009.

[59] A. Roine. HSC Chemistry® [Software], Outotec, Pori 2018. Software available at www.outotec.com/HSC (accessed on 25.03.2021).

[60] Davies RH, Dinsdale AT, Gisby JA, Robinson JAJ, Martin SM. MTDATA - thermodynamic and phase equilibrium software from the national physical laboratory. Calphad 2002;26(2):229–71. https://doi.org/10.1016/S0364-5916(02)00036-6.

[61] Andersson J-O, Helander T, Höglund L, Shi P, Sundman B. Thermo-Calc & DICTRA, computational tools for materials science. Calphad 2002;26(2): 273–312. https://doi.org/10.1016/S0364-5916(02)00037-8.

[62] Lindberg D, Backman R, Chartrand P, Hupa M. Towards a comprehensive thermodynamic database for ash-forming elements in biomass and waste combustion — Current situation and future developments. Fuel Process Technol 2013;105:129–41. https://doi.org/10.1016/j.fuproc.2011.08.008.

[63] Thy P, Jenkins BM, Lesher CE, Grundvig S. Compositional constraints on slag formation and potassium volatilization from rice straw blended wood fuel. Fuel Process Technol 2006;87(5):383–408. https://doi.org/10.1016/j.fuproc.2005.08.015.

[64] Carmona VB, Oliveira RM, Silva WTL, Mattoso LHC, Marconcini JM. Nanosilica from rice husk: Extraction and characterization. Ind Crops Prod 2013;43:291–6. https://doi.org/10.1016/j.indcrop.2012.06.050.

[65] Zareihassangheshlaghi A, Beidaghy Dizaji H, Zeng T, Huth P, Ruf T, Denecke R, et al. Behavior of Metal Impurities on Surface and Bulk of Biogenic Silica from Rice Husk Combustion and the Impact on Ash-Melting Tendency. ACS Sustainable Chem. Eng. 2020;8(28):10369–79. https://doi.org/10.1021/acssuschemeng.0c0148410.1021/acssuschemeng.0c01484.s001.

[66] Alyosef HA, Eilert A, Welscher J, Ibrahim SS, Denecke R, Schwieger W, et al. Characterization of biogenic silica generated by thermo chemical treatment of rice husk. Part Sci Technol 2013;31(5):524–32. https://doi.org/10.1080/02726351.2013.782931.

[67] Yalçin N, Sevinç V. Studies on silica obtained from rice husk. Ceram Int 2001;27 (2):219–24. https://doi.org/10.1016/S0272-8842(00)00068-7.

[68] Maseko NN, Schneider D, Wassersleben S, Enke D, Iwarere SA, Pocock J, et al. The Production of Biogenic Silica from Different South African Agricultural Residues through a Thermo-Chemical Treatment Method. Sustainability 2021;13 (2):577. https://doi.org/10.3390/su13020577.

[69] Umeda J, Kondoh K. High-purification of amorphous silica originated from rice husks by combination of polysaccharide hydrolysis and metallic impurities removal. Ind Crops Prod 2010;32(3):539–44. https://doi.org/10.1016/j.indcrop.2010.07.002.

[70] Schliermann T, Hartmann I, Beidaghy Dizaji H, Zeng T, Schneider D, Wassersleben S, et al. High quality biogenic silica from combined energetic and material utilization of agricultural residues. In: 7th International Symposium of Energy from Biomass and Waste. 2018.

[71] DHHS, Department of Health and Human Services, Centers for Disease Control and Prevention. Health Effects of Occupational Exposure to Respirable Crystalline Silica, DHHS (NIOSH) Publication No. 2002-129, 2002.

[72] Rice F, Park R, Stayner L, Smith R, Gilbert S, Checkoway H. Crystalline silica exposure and lung cancer mortality in diatomaceous earth industry workers: A quantitative risk assessment. Occupat. environ. medicine 2001;58:38–45.

[73] Chen P, Gu W, Fang W, Ji X, Bie R. Removal of metal impurities in rice husk and characterization of rice husk ash under simplified acid pretreatment process. Environ. Prog. Sustainable Energy 2017;36(3):830–7. https://doi.org/10.1002/ep.v36.310.1002/ep.12513.

[74] Chandrasekhar S, Pramada PN, Praveen L. Effect of organic acid treatment on the properties of rice husk silica. J Mater Sci 2005;40(24):6535–44. https://doi.org/10.1007/s10853-005-1816-z.

[75] Chakraverty A, Mishra P, Banerjee HD. Investigation of combustion of raw and acid-leached rice husk for production of pure amorphous white silica. J Mater Sci 1988;23(1):21–4. https://doi.org/10.1007/BF01174029.

[76] Umeda J, Kondoh K, Michiura Y. Process Parameters Optimization in Preparing High-Purity Amorphous Silica Originated from Rice Husks. Mater. Trans. 2007;48 (12):3095–100. https://doi.org/10.2320/matertrans.MK200715.

[77] Mack R, Kuptz D, Schön C, Hartmann H. Combustion behavior and slagging tendencies of kaolin additivated agricultural pellets and of wood-straw pellet blends in a small-scale boiler. Biomass Bioenergy 2019;125(3):50–62. https://doi.org/10.1016/j.biombioe.2019.04.003.

[78] Schön C, Feldmeier S, Hartmann H, Schwabl M, Dahl J, Rathbauer J, et al. New Experimental Evaluation Strategies Regarding Slag Prediction of Solid Biofuels in Pellet Boilers. Energy Fuels 2019;33(11):11985–95. https://doi.org/10.1021/acs.energyfuels.9b03098.

[79] Deutsches Institut für Normung. DIN EN ISO 17225–1, Solid biofuels – Fuel specifications and classes – Part 1: General requirements. Berlin: Germany, Beuth Verlag; 2014. https://doi.org/10.31030/2073606.

[80] Deutsches Institut für Normung. DIN EN ISO 18122. Biogene Festbrennstoffe - Bestimmung des Aschegehaltes. Berlin: Germany, Beuth Verlag; 2016. https://doi.org/10.31030/2316155.

[81] Zevenhoven-Onderwater M. Ash-forming matter in biomass fuels [PhD thesis]. Finland: Department of Chemical Engineering. Åbo Akademi University; 2001.

[82] International Organization for Standardization, ISO 16948, Solid biofuels - Determination of total content of carbon, hydrogen and nitrogen, 2015.

[83] Deutsches Institut für Normung. DIN EN 15935, Schlamm, behandelter Bioabfall, Boden und Abfall - Bestimmung des Glühverlusts; Deutsche und Englische Fassung prEN. Berlin, Germany, Beuth Verlag, 2020. https://doi.org/10.31030/3134550.

[84] de Caro CA, Aichert A, Walter CM. Efficient, precise and fast water determination by the Karl Fischer titration. Food Control 2001;12(7):431–6. https://doi.org/10.1016/S0956-7135(01)00020-2.

[85] Gualtieri AF. Accuracy of XRPD QPA using the combined Rietveld–RIR method. J Appl Crystallogr 2000;33(2):267–78. https://doi.org/10.1107/S002188989901643X.

[86] Young RA, editor. The Rietveld Method. International Union of Crystallography. Oxford University Press; 1993.

[87] Unifit Scientific Software GmbH, Leipzig, www: https://unifit-software.de.

[88] Brunauer S, Emmett PH, Teller E. Adsorption of gases in multimolecular layers. J. Am. Chem. Soc. 1938;60(2):309–19. https://doi.org/10.1021/ja01269a023.

[89] Webb PA, Orr C. Analytical methods in fine particle technology. 1st ed. Norcross: Micromeritics; 1997.

[90] Schneider D, Wassersleben S, Weiß M, Denecke R, Stark A, Enke D. A Generalized Procedure for the Production of High-Grade. Porous Biogenic Silica. Waste Biomass Valor 2020;11(1):1–15. https://doi.org/10.1007/s12649-018-0415-6.

[91] Deutsches Institut für Normung. DIN EN ISO 16967, Biogene Festbrennstoffe - Bestimmung von Hauptelementen - Al, Ca, Fe, Mg, P, K, Si. Na und Ti. Berlin: Germany, Beuth Verlag; 2015. https://doi.org/10.31030/2266314.

[92] Duchesne MA, Bronsch AM, Hughes RW, Masset PJ. Slag viscosity modeling toolbox. Fuel 2013;114:38–43. https://doi.org/10.1016/j.fuel.2012.03.010.

[93] Momma K, Izumi F. VESTA 3 for three-dimensional visualization of crystal, volumetric and morphology data. J Appl Crystallogr 2011;44(6):1272–6. https://doi.org/10.1107/S0021889811038970.

[94] Blander M, Pelton AD. Thermodynamic analysis of binary liquid silicates and prediction of ternary solution properties by modified quasichemical equations. Geochim Cosmochim Acta 1987;51(1):85–95. https://doi.org/10.1016/0016-7037(87)90009-3.

[95] Sommersacher P, Brunner T, Obernberger I, Kienzl N, Kanzian W. Application of Novel and Advanced Fuel Characterization Tools for the Combustion Related Characterization of Different Wood/Kaolin and Straw/Kaolin Mixtures. Energy Fuels 2013;27(9):5192–206. https://doi.org/10.1021/ef400400n.

[96] Doshi V, Vuthaluru HB, Korbee R, Kiel JHA. Development of a modeling approach to predict ash formation during co-firing of coal and biomass. Fuel Process Technol 2009;90(9):1148–56. https://doi.org/10.1016/j.fuproc.2009.05.019.

[97] Magdziarz A, Gajek M, Nowak-Woźny D, Wilk M. Mineral phase transformation of biomass ashes – Experimental and thermochemical calculations. Renewable Energy 2018;128:446–59. https://doi.org/10.1016/j.renene.2017.05.057.

[98] Vassilev SV, Baxter D, Vassileva CG. An overview of the behaviour of biomass during combustion: Part I. Phase-mineral transformations of organic and inorganic matter. Fuel 2013;112(3):391–449. https://doi.org/10.1016/j.fuel.2013.05.043.

[99] He F, Li X, Behrendt F, Schliermann T, Shi J, Liu Y. Critical changes of inorganics during combustion of herbaceous biomass displayed in its water soluble fractions. Fuel Process Technol 2020;198(1–3):106231. https://doi.org/10.1016/j.fuproc.2019.106231.

[100] Nguyen MN, Dultz S, Picardal F, Bui ATK, van Pham Q, Schieber J. Release of potassium accompanying the dissolution of rice straw phytolith. Chemosphere 2015;119:371–6. https://doi.org/10.1016/j.chemosphere.2014.06.059.

[101] Crawford MD. Hardness of drinking-water and cardiovascular disease. Proc Nutr Soc 1972;31(3):347–53. https://doi.org/10.1079/PNS19720062.

[102] van Loo S, Koppejan J, editors. The handbook of biomass combustion and co-firing. London: Earthscan; 2008.

[103] Niu Y, Du W, Tan H, Xu W, Liu Y, Xiong Y, et al. Further study on biomass ash characteristics at elevated ashing temperatures: The evolution of K, Cl, S and the ash fusion characteristics. Bioresour Technol 2013;129:642–5. https://doi.org/10.1016/j.biortech.2012.12.065.

[104] Priscak J, Kuba M, Hofbauer H. Development of a New Method for Investigation of the Ash Melting Behavior in the Fluidized Bed Conversion Processes; 2019; Available from: http://hdl.handle.net/20.500.12708/15384.

[105] Dahou T. Contribution to the understanding of the role of inorganic elements in biomass steam gasification. Chemical and Process Engineering. Université Grenoble Alpes 2019.

[106] Ma X, Ren T, Kong D, Nie Y, Pang M, Xu J, et al. Experiments on mechanism of biomass ash slagging. In: In: 2011 International Conference on Electric Information and Control Engineering. IEEE; 2011. p. 5031–4.

[107] Alyosef HA. Rice Husk ash (RHA) as a Renewable Source for Value Added Silica: Products the Way to Standardized Educts, Comprehensive Characterization, Modification and Phase Transformation. Ph.D. Thesis, Universität Leipzig, Leipzig, Germany, 2014.

[108] Shaw HR. Viscosities of magmatic silicate liquids; an empirical method of prediction. Am J Sci 1972;272(9):870–93. https://doi.org/10.2475/ajs.272.9.870.

[109] Hui H. Viscosity of silicate melts [Doctor of Philosophy]. USA: The University of Michigan; 2008.

[110] Onodera Y, Takimoto Y, Hijiya H, Taniguchi T, Urata S, Inaba S, et al. Origin of the mixed alkali effect in silicate glass. NPG Asia Mater 2019;11(1). https://doi.org/10.1038/s41427-019-0180-4.

[111] Roy PK, Heyde M, Heuer A. Modelling the atomic arrangement of amorphous 2D silica: A network analysis. Phys Chem Chem Phys 2018;20(21):14725–39. https://doi.org/10.1039/C8CP01313F.

[112] Lunt AJG, Chater P, Korsunsky AM. On the origins of strain inhomogeneity in amorphous materials. Sci Rep 2018;8(1):1574. https://doi.org/10.1038/s41598-018-19900-2.

[113] Callister Jr. WD, Rethwisch DG. Materials Science and Engineering: An Introduction. 10th ed. John Wiley & Sons.

[114] Brito LBQ, Brito GF, Morais CRS. Alternative for fine pure silica in kiln-casting glass molds. Mater Lett 2019;252:19–22. https://doi.org/10.1016/j.matlet.2019.05.048.

[115] Wan W, Luo J, Yang J, Feng Y, Ouyang Y, Chen D, et al. High-temperature ablation properties of nano zirconia reinforced fused silica ceramics. Ceram Int 2018;44(6):7273–5. https://doi.org/10.1016/j.ceramint.2018.01.186.

[116] Bottinga Y, Richet P. Thermodynamics of liquid silicates, a preliminary report. Earth Planet Sci Lett 1978;40(3):382–400. https://doi.org/10.1016/0012-821X(78)90161-9.

[117] Deng X, Yang W, Liu XQ, Cheng BJ, Liu T. Study on Properties of Wollastonite Micro Fiber Reinforced Mortar. AMR 2013;785–786:151–6. https://doi.org/10.4028/www.scientific.net/AMR.785-786.151.

[118] Sai Nikhil P, Ravichandran PT, Divya KK. Stabilisation and characterisation of soil using wollastonite powder. Mater Today: Proc 2020;8(143):714. https://doi.org/10.1016/j.matpr.2020.05.489.

[119] Zareei SA, Ameri F, Shoaei P, Bahrami N. Recycled ceramic waste high strength concrete containing wollastonite particles and micro-silica: A comprehensive experimental study. Constr Build Mater 2019;201:11–32. https://doi.org/10.1016/j.conbuildmat.2018.12.161.

[120] Bian H, Hannawi K, Takarli M, Molez L, Prince W. Effects of thermal damage on physical properties and cracking behavior of ultrahigh-performance fiber-reinforced concrete. J Mater Sci 2016;51(22):10066–76. https://doi.org/10.1007/s10853-016-0233-9.

[121] Barin I, Knacke O, Kubaschewski O, editors. Thermochemical properties of inorganic substances. Berlin, Heidelberg: Springer Berlin Heidelberg; 1977.

[122] Mysen BO, Virgo D. In: Advanced Mineralogy. Berlin, Heidelberg: Springer Berlin Heidelberg; 1994. p. 238–54. https://doi.org/10.1007/978-3-642-78523-8_14.

[123] Okada K, Kameshima Y, Yasumori A. Chemical Shifts of Silicon X-ray Photoelectron Spectra by Polymerization Structures of Silicates. J Am Ceram Soc 1998;81(7):1970–2. https://doi.org/10.1111/j.1151-2916.1998.tb02579.x.

[124] Xuan W, Wang H, Xia D. Depolymerization mechanism of CaO on network structure of synthetic coal slags. Fuel Process Technol 2019;187:21–7. https://doi.org/10.1016/j.fuproc.2019.01.005.
[125] Yazhenskikh E, Hack K, Müller M. Critical thermodynamic evaluation of oxide systems relevant to fuel ashes and slags. Part 1: Alkali oxide–silica systems. Calphad 2006;30(3):270–6. https://doi.org/10.1016/j.calphad.2006.03.003.
[126] Gutiérrez-Castorena MdelC, Effland WR. In: Interpretation of Micromorphological Features of Soils and Regoliths. Elsevier; 2010. p. 471–96. https://doi.org/10.1016/B978-0-444-53156-8.00021-0.
[127] Vargas S, Frandsen FJ, Dam-Johansen K. Rheological properties of high-temperature melts of coal ashes and other silicates. Prog Energy Combust Sci 2001;27(3):237–429. https://doi.org/10.1016/S0360-1285(00)00023-X.
[128] Hess PC. Polymer model of silicate melts. Geochim Cosmochim Acta 1971;35(3):289–306. https://doi.org/10.1016/0016-7037(71)90038-X.
[129] Falk J, Skoglund N, Grimm A, Öhman M. Fate of phosphorus in fixed bed combustion of biomass and sewage sludge. Energy Fuels 2020;34(4):4587–94. https://doi.org/10.1021/acs.energyfuels.9b03976.
[130] Stemann J, Peplinski B, Adam C. Thermochemical treatment of sewage sludge ash with sodium salt additives for phosphorus fertilizer production–Analysis of underlying chemical reactions. Waste Manag 2015;45:385–90. https://doi.org/10.1016/j.wasman.2015.07.029.
[131] Ma C, Weiland F, Hedman H, Boström D, Backman R, Öhman M. Characterization of Reactor Ash Deposits from Pilot-Scale Pressurized Entrained-Flow Gasification of Woody Biomass. Energy Fuels 2013;27(11):6801–14. https://doi.org/10.1021/ef401591a.
[132] Li F, Li Y, Fan H, Wang T, Guo M, Fang Y. Investigation on fusion characteristics of deposition from biomass vibrating grate furnace combustion and its modification. Energy 2019;174(11):724–34. https://doi.org/10.1016/j.energy.2019.02.154.
[133] Lindström E, Öhman M, Backman R, Boström D. Influence of Sand Contamination on Slag Formation during Combustion of Wood Derived Fuels. Energy Fuels 2008;22(4):2216–20. https://doi.org/10.1021/ef700772q.
[134] U.S. Department of the Interior. Geological Survey Bulletin, Geological Survey; Washington, D.C., 1949.
[135] Thy P, Lesher CE, Jenkins BM. Experimental determination of high-temperature elemental losses from biomass slag. Fuel 2000;79(6):693–700. https://doi.org/10.1016/S0016-2361(99)00195-7.
[136] Bahrami A, Simon U, Soltani N, Zavareh S, Schmidt J, Pech-Canul MI, et al. Eco-fabrication of hierarchical porous silica monoliths by ice-templating of rice husk ash. Green Chem. 2017;19(1):188–95. https://doi.org/10.1039/C6GC02153K.
[137] Chen M, Zhao B. Viscosity measurements of the SiO2–K2O–CaO system relevant to biomass slags. Fuel 2016;180:638–44. https://doi.org/10.1016/j.fuel.2016.04.099.
[138] Ma C, Skoglund N, Carlborg M, Broström M. Viscosity of molten CaO K2O SiO2 woody biomass ash slags in relation to structural characteristics from molecular dynamics simulation. Chem Eng Sci 1997;2020(215):115464. https://doi.org/10.1016/j.ces.2019.115464.